NASA/TP-2010-216856

Comparison of Damage Models for Predicting the Non-linear Response of Laminates Under Matrix Dominated Loading Conditions

Clara Schuecker
LUXNER Composite Simulation, Vienna, Austria

Carlos G. Dávila and Cheryl A. Rose
Langley Research Center, Hampton, Virginia

October 2010

NASA STI Program . . . in Profile

Since its founding, NASA has been dedicated to the advancement of aeronautics and space science. The NASA scientific and technical information (STI) program plays a key part in helping NASA maintain this important role.

The NASA STI program operates under the auspices of the Agency Chief Information Officer. It collects, organizes, provides for archiving, and disseminates NASA's STI. The NASA STI program provides access to the NASA Aeronautics and Space Database and its public interface, the NASA Technical Report Server, thus providing one of the largest collections of aeronautical and space science STI in the world. Results are published in both non-NASA channels and by NASA in the NASA STI Report Series, which includes the following report types:

- TECHNICAL PUBLICATION. Reports of completed research or a major significant phase of research that present the results of NASA programs and include extensive data or theoretical analysis. Includes compilations of significant scientific and technical data and information deemed to be of continuing reference value. NASA counterpart of peer-reviewed formal professional papers, but having less stringent limitations on manuscript length and extent of graphic presentations.

- TECHNICAL MEMORANDUM. Scientific and technical findings that are preliminary or of specialized interest, e.g., quick release reports, working papers, and bibliographies that contain minimal annotation. Does not contain extensive analysis.

- CONTRACTOR REPORT. Scientific and technical findings by NASA-sponsored contractors and grantees.

- CONFERENCE PUBLICATION. Collected papers from scientific and technical conferences, symposia, seminars, or other meetings sponsored or co-sponsored by NASA.

- SPECIAL PUBLICATION. Scientific, technical, or historical information from NASA programs, projects, and missions, often concerned with subjects having substantial public interest.

- TECHNICAL TRANSLATION. English-language translations of foreign scientific and technical material pertinent to NASA's mission.

Specialized services also include creating custom thesauri, building customized databases, and organizing and publishing research results.

For more information about the NASA STI program, see the following:

- Access the NASA STI program home page at *http://www.sti.nasa.gov*

- E-mail your question via the Internet to help@sti.nasa.gov

- Fax your question to the NASA STI Help Desk at 443-757-5803

- Phone the NASA STI Help Desk at 443-757-5802

- Write to:
  NASA STI Help Desk
  NASA Center for AeroSpace Information
  7115 Standard Drive
  Hanover, MD 21076-1320

NASA/TP-2010-216856

Comparison of Damage Models for Predicting the Non-linear Response of Laminates Under Matrix Dominated Loading Conditions

Clara Schuecker
LUXNER Composite Simulation, Vienna, Austria

Carlos G. Dávila and Cheryl A. Rose
Langley Research Center, Hampton, Virginia

National Aeronautics and
Space Administration

Langley Research Center
Hampton, Virginia 23681-2199

October 2010

Available from:

NASA Center for AeroSpace Information
7115 Standard Drive
Hanover, MD 21076-1320
443-757-5802

Comparison of damage models for predicting the non-linear response of laminates under matrix dominated loading conditions

Clara Schuecker[1], Carlos G. Dávila[2] and Cheryl A. Rose[2]

[1] *LUXNER Composite Simulation, Vienna, Austria*

[2] *NASA Langley Research Center, Hampton, VA 23681*

Abstract

Five models for matrix damage in fiber reinforced laminates previously presented in the literature are evaluated for matrix dominated loading conditions under plane stress (i.e. tension transverse to fibers combined with in-plane shear) and are compared both qualitatively and quantitatively. The emphasis of this study is on modeling the response of embedded plies to homogeneous stress states rather than localized failure caused by stress concentrations (e.g. at notches). Three of the models are specifically designed for modeling the non-linear response due to distributed matrix cracking under homogeneous loading, and also account for non-linear (shear) behavior prior to the onset of cracking. The remaining two models are localized damage models intended for predicting local failure at stress concentrations. These last two models are not strictly applicable to the test cases considered here but, nevertheless, are also included in this study for comparison and to point out qualitative differences in the various modeling strategies.

In this study, the modeling approaches of distributed vs. localized cracking as well as the different formulations of damage initiation and damage progression are discussed. In addition, the following issues are addressed:

- stress-strain response of an embedded ply under transverse tension,
- damage initiation,
- anisotropy of property degradation due to damage,
- non-linearity prior to damage onset (plasticity).

Key words: Fiber Reinforced Laminates, Polymer Matrix Composites, Computational Mechanics, Non-Linear Modeling, Continuum Damage, Plasticity.

Notation

Indices:

1, 2, 3	...	ply coordinates (1 – fiber, 2 – transverse in-plane, 3 – out-of-plane direction)
l, n, t	...	fracture plane coordinates (l – fiber, n – normal, t – transverse direction)
x, y, z	...	global coordinates (x – loading direction, y – transverse to load, in plane, z – out of plane)

Greek letters:

β	...	lay-up angle for off-axis plies
γ_{ij}	...	engineering shear strain on plane i in direction j
$\gamma_{ij}^{\mathrm{pl}}$	...	plastic shear strain on plane i in direction j
$\Delta U/width$	...	energy dissipated by the creation of a new crack
δ_{eq}	...	equivalent displacement (`ABAQUS` model)
δ_{eq}^{0}	...	equivalent displacement at damage onset (`ABAQUS` model)
$\delta_{\mathrm{eq}}^{\mathrm{f}}$	...	equivalent displacement at final failure (`ABAQUS` model)
$\boldsymbol{\varepsilon}$	...	strain tensor
ε_{ii}	...	normal strain component on plane i in direction i
$\boldsymbol{\varepsilon}^{\mathrm{pl}}$	...	plastic strain tensor
$\varepsilon_{\mathrm{eq}}$	...	equivalent strain (*constant stress* model)
η_{L}	...	slope parameter for LaRC 04 criterion
κ	...	damage evolution parameter (*Mori-Tanaka* model)
ν_{12}	...	major in-plane Poisson's ratio
ν_{21}	...	minor in-plane Poisson's ratio ($\nu_{21} = \nu_{12}\, E_2/E_1$)
$\boldsymbol{\sigma}$	...	ply stress tensor
σ_{ij}	...	stress component on plane i in direction j
σ_{ij}^{0}	...	stress component at damage onset on plane i in direction j
$\hat{\boldsymbol{\sigma}}$	...	effective stress tensor (`ABAQUS` model)
$\boldsymbol{\sigma}^{\mathrm{eff}}$	...	effective stress tensor (*constant stress* and *periodic crack* model)
σ^{eff}	...	magnitude of effective stress tensor
$\sigma_{ij}^{\mathrm{eff}}$	...	effective stress component on plane i in direction j
σ_{fp}	...	fracture plane stress (magnitude of fracture plane traction vector)
σ_{fp}^{0}	...	fracture plane stress at damage onset
θ_{fp}	...	fracture plane angle
χ	...	shear response factor (*periodic crack* model)

Roman letters:

CD	...	crack density
CD^{sat}	...	crack density at saturation
d_{f}	...	damage variable for fiber failure (`ABAQUS` model)
d_{m}	...	damage variable for matrix failure (`ABAQUS` model)
d_{s}	...	damage variable for shear failure (`ABAQUS` model)
$\boldsymbol{E}^{\mathrm{d}}$	...	elasticity tensor of a damaged ply
$\boldsymbol{E}_{\mathrm{Lam}}$	...	elasticity tensor of a laminate (*periodic crack* model)
E_i	...	Young's modulus of a ply in i-direction
E_i^{d}	...	Young's modulus of a damaged ply in i-direction
E_2^0	...	Young's modulus of an undamaged ply in transverse direction
E_2^{sec}	...	secant Young's modulus in transverse direction
e_{n}	...	inclusion aspect ratio (*Mori-Tanaka* damage model)
f_{12}	...	non-linear function, in-plane shear (*constant stress* model)
f_2	...	non-linear function, transverse tension (*constant stress* model)
FI	...	failure index
G_{12}	...	in-plane shear modulus of a ply
G_{12}^0	...	shear modulus of an undamaged ply
G_{12}^{sec}	...	secant shear modulus
$G_{\mathrm{Ic,ply}}$	...	critical energy release rate for intra-ply cracking in mode I
$G_{\mathrm{IIc,ply}}$	...	critical energy release rate for intra-ply cracking in mode II
$G_{\mathrm{c,ply}}$	...	critical energy release rate for intra-ply cracking (mixed mode)
h_{ges}	...	half thickness of laminate (*periodic crack* model)
h_{90}	...	half thickness of 90° ply-stack (*periodic crack* model)
k	...	parameter of shear plasticity law (*Mori-Tanaka* model)
L	...	half distance between two cracks (*periodic crack* model)
L_{ch}	...	characteristic length (*exponential softening* and `ABAQUS` model)
L^{sat}	...	half distance between two cracks at crack saturation
n	...	exponent of shear plasticity law (*Mori-Tanaka* model)
p_{12}^{t}	...	slope parameter for Puck failure criterion
S	...	in-situ shear strength
S^{IF}	...	interlaminar shear strength
U^{dis}	...	dissipated energy density
U^{sat}	...	dissipated energy density at crack saturation
t	...	thickness of a cluster of equally oriented plies
$Y_{\mathrm{linear}}^{\mathrm{t}}$	...	in-situ transverse tensile strength (linear material)
$Y_{\mathrm{non\text{-}linear}}^{\mathrm{t}}$	...	in-situ transverse tensile strength (non-linear material)

1 INTRODUCTION

Fiber reinforced composites are being increasingly used in applications that require lightweight design. In order to achieve further weight reductions without compromising the reliability of composite parts, accurate prediction of the material response including non-linear behavior is beneficial. Models for predicting the non-linear response of laminates are typically formulated on the ply level and distinguish between various failure modes in order to capture the different effects of those failure modes appropriately.

In polymer matrix composites, the first failure modes that are normally observed are dominated by the matrix constituent. These failure modes affect the response of a ply, and may lead to a non-linear stress–strain relation, but in most cases do not lead to complete laminate failure. Depending on the kind of loading, the failure modes that can be observed are matrix cracking and matrix plasticity. Many models for predicting the non-linear response of an embedded ply have been proposed in the literature. While most of the models focus on stiffness degradation due to matrix cracking (e.g. 1 – 9) some also include non-linearity caused by matrix plasticity (e.g. 10 – 12).

In the present work, five damage models that have recently been presented in the literature are evaluated [5, 7, 9, 11, 12]. The models were chosen to provide a sample of different approaches that are representative of the state of the art in damage modeling. The first three damage models include formulations for non-linearity due to matrix plasticity and to progressive matrix cracking [5, 11, 12]. The remaining two models include non-linearity due to localized progressive matrix cracking only [7, 9]. A brief description of each model is presented, followed by a general discussion on modeling issues, such as distributed vs. localized cracking and different formulations of damage initiation and damage progression. Finally, predictions from these models using the same set of input data are compared, qualitatively and quantitatively, to experimental data from the literature, evaluating their ability to accurately predict the change in laminate axial stiffness and Poisson's ratio as a function of applied strain. The objective of this comparison is to point out the respective features and differences of the various models regarding plasticity, damage initiation, and property degradation due to damage, and also to provide some guidelines with respect to the applicability of different modeling strategies to a given problem.

A state of plane stress is assumed throughout this study even though some of the models can also be applied to triaxial stress states. Furthermore, the discussions here are focused on loading scenarios that lead to a combination of transverse tension and in-plane shear stresses in each ply. According to ply failure criteria that are based on Mohr's fracture hypothesis for brittle mate-

rials such as the Puck criterion [13] and the LaRC 04 criterion [14], such stress states cause matrix cracks that are perpendicular to the laminate plane. Damage due to inclined matrix cracks, which occur under transverse compression, are not investigated here. Finally, it is noted that the laminates studied here were designed to emphasize the effect of matrix damage such that it could be studied properly. Laminates for practical applications usually have more evenly distributed fiber directions (e.g. quasi-isotropic laminates) and thinner ply groups, so the effect of matrix cracking on laminate stiffness is typically smaller.

2 OVERVIEW OF MODELS

In this section, the damage models considered in this study are summarized. The general idea and basic assumptions of the models are explained, rather than providing complete model definitions. For detailed information on the model formulations, see the respective references.

2.1 Damage / plasticity model using Mori-Tanaka approach

The *'MoriT'* model proposed by Schuecker *et al.* [10, 11] is a constitutive model specifically for matrix-dominated non-linearities in plane stress. It includes non-linearity due to progressive matrix cracking and matrix plasticity, while damage due to fiber failure modes is not taken into account. Instead, fiber failure is considered as the ultimate failure. The damage and plasticity laws used in the model are both formulated with respect to a fracture plane that is parallel to the fiber direction and defined by the angle θ_{fp} (see Fig.1). The fracture plane orientation is predicted by the Puck failure criterion for plane stress states [13, 15, 16].

Plastic strain is assumed to be driven by the shear stress in the fracture plane (i.e. the projection of the traction vector onto the fracture plane) and to follow the direction of the fracture plane's shear stress vector. Therefore, the only

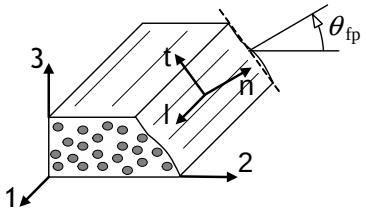

Fig. 1. Definition of fracture plane and corresponding coordinate system, l-n-t, with regard to the ply coordinate system, 1-2-3, by fracture plane angle, θ_{fp}.

non-zero contributions to plastic strain, when referenced to the fracture plane coordinates l–n–t, are the shear strain components

$$\begin{aligned} \gamma_{\mathsf{ln}}^{\mathrm{pl}} &= f\left(\sigma_{\mathsf{ln}} = \sigma_{12}\cos\theta_{\mathrm{fp}}\right) \\ \gamma_{\mathsf{nt}}^{\mathrm{pl}} &= f\left(\sigma_{\mathsf{nt}} = -\sigma_{22}\cos\theta_{\mathrm{fp}}\sin\theta_{\mathrm{fp}}\right) \quad . \end{aligned} \tag{1}$$

For the load cases considered in this study, the Puck failure criterion predicts a perpendicular fracture plane ($\theta_{\mathrm{fp}} = 0$). This means that the fracture plane coordinate system coincides with the ply coordinate system (cf. Fig.1), leaving the in-plane shear strain as the only non-zero component of the plastic strain tensor ($\gamma_{12}^{\mathrm{pl}} = \gamma_{\mathsf{ln}}^{\mathrm{pl}}$). The relation $\gamma_{12}^{\mathrm{pl}} = f(\sigma_{12})$ is determined by analytical curve fitting to experimental data.

Damage onset and damage evolution are controlled by the failure index computed from the Puck failure criterion. The stresses used to evaluate the Puck criterion are the nominal (homogenized) stresses in the ply and are computed as

$$\boldsymbol{\sigma} = \boldsymbol{E}^{\mathrm{d}} : (\boldsymbol{\varepsilon} - \boldsymbol{\varepsilon}^{\mathrm{pl}}) \quad , \tag{2}$$

where $\boldsymbol{\varepsilon}$ is the given strain tensor, $\boldsymbol{\varepsilon}^{\mathrm{pl}}$ is the plastic strain tensor determined by the plasticity law, and $\boldsymbol{E}^{\mathrm{d}}$ is the elasticity tensor of the damaged material. The elasticity tensor $\boldsymbol{E}^{\mathrm{d}}$ is computed by the Mori-Tanaka method [17] using penny shaped inclusions which are aligned with the predicted fracture plane. The increase of damage is controlled by increasing the volume fraction of voids in the Mori-Tanaka formulation according to an empirical evolution law that relates the volume fraction to the failure index, *FI*, of the Puck criterion. Due to the formulation of the evolution law proposed in [11], damage onset occurs before the failure envelope is reached at the failure index $FI = \frac{1}{1+\kappa}$ depending on the evolution parameter, κ. Since *FI* is a function of the stress state, the elasticity tensor (as well as the plastic strain tensor) implicitly depends on the stress tensor $\boldsymbol{\sigma}$. The constitutive equation, Eq. (2), therefore needs to be solved iteratively to compute $\boldsymbol{\sigma}$, $\boldsymbol{\varepsilon}^{\mathrm{pl}}(\boldsymbol{\sigma})$ and $\boldsymbol{E}^{\mathrm{d}}(\boldsymbol{\sigma})$ for a given strain state, $\boldsymbol{\varepsilon}$.

2.2 Damage / plasticity model assuming constant stress

The *'ConStress'* model proposed by Pinho *et al.* [12] is applicable to triaxial stress states and includes effects of all currently known failure processes such as matrix cracking, matrix plasticity, fiber rupture, fiber kinking, and delamination. Additionally, it takes into account the influence of hydrostatic stresses on elastic properties and fiber kinking. In the present study, only matrix cracking and matrix plasticity are considered. Furthermore, only plane stress states are investigated and the change of elastic properties due to hydrostatic stress is therefore neglected.

Non-linearity prior to damage onset, which is caused by matrix plasticity, is described by the change of secant shear modulus and secant transverse Young's modulus as functions of an equivalent strain (defined here for plane stress)

$$\begin{aligned} &E_2^{\mathrm{sec}}/E_2^0 = f_2(\varepsilon_{\mathrm{eq}}), \qquad G_{12}^{\mathrm{sec}}/G_{12}^0 = f_{12}(\varepsilon_{\mathrm{eq}}) \\ &\text{where} \quad \varepsilon_{\mathrm{eq}} = \sqrt{(\varepsilon_{22}-\varepsilon_{33})^2 + \gamma_{12}^2} \quad . \end{aligned} \tag{3}$$

The functions $f_2(\varepsilon_{\mathrm{eq}})$ and $f_{12}(\varepsilon_{\mathrm{eq}})$ need to be determined from experimental data of the corresponding uniaxial tests either by point wise interpolation or analytical curve fits.

The failure criterion used to predict the onset of matrix cracking is a modified version of the Mohr-Coulomb failure criterion adapted for uni-directional composites. Similarly to the Puck failure criterion, this criterion predicts the fracture plane orientation, θ_{fp}, in addition to the failure index. Onset and propagation of damage are controlled by an effective stress tensor defined as

$$\boldsymbol{\sigma}^{\mathrm{eff}} = \boldsymbol{E}^0 : (\boldsymbol{\varepsilon} - \boldsymbol{\varepsilon}^{\mathrm{pl}}) \quad , \tag{4}$$

where $\boldsymbol{E}^0$ denotes the initial elasticity tensor of the undamaged ply material and $\boldsymbol{\varepsilon}^{\mathrm{pl}}$ is the strain tensor resulting from the plasticity formulation in Eq. (3). For perpendicular fracture planes ($\theta_{\mathrm{fp}} = 0$), the transverse Young's modulus and the shear modulus are degraded in such a way that the nominal stress on the fracture plane, σ_{fp} (defined as the magnitude of the fracture plane's traction vector), remains constant after damage onset, i.e.

$$\begin{aligned} &E_2^{\mathrm{d}} = (1-d)E_2^{\mathrm{sec}}, \quad G_{12}^{\mathrm{d}} = (1-d)G_{12}^{\mathrm{sec}} \\ &\text{where} \quad d = 1 - \frac{\sigma_{\mathrm{fp}}^0}{\sigma^{\mathrm{eff}}} \\ &\text{and} \quad \sigma_{\mathrm{fp}}^0 = \sqrt{(\sigma_{22}^0)^2 + (\sigma_{12}^0)^2}, \quad \sigma^{\mathrm{eff}} = \sqrt{(\sigma_{22}^{\mathrm{eff}})^2 + (\sigma_{12}^{\mathrm{eff}})^2} \quad , \end{aligned} \tag{5}$$

where σ_{fp}^0 denotes the magnitude of the fracture plane traction vector at damage onset. No additional non-linearity due to plasticity is assumed after damage onset. Therefore, $\boldsymbol{\varepsilon}^{\mathrm{pl}}$ does not change during damage accumulation and since $\boldsymbol{E}^0$ is constant, the effective stress and the ensuing stiffness degradation can be computed explicitly from Eqs. (4) and (5) for a given strain state, $\boldsymbol{\varepsilon}$.

2.3 Periodic damage model

The periodic damage model, *'PerCrack'* [6, 18], focuses on the prediction of transverse matrix cracks. The model is based on an analytical solution proposed by Tan and Nuismer [19, 20], which relates the elasticity tensor of a laminate consisting of a 90°-ply embedded between two orthotropic sub-

laminates, S, to the density of periodically arranged matrix cracks in the 90°-ply (see Fig. 2). Strictly speaking, the model is therefore restricted to laminates that have a $(S/90_n)_\mathrm{s}$ lay-up and in its original version can only be applied for either uniaxial tension or in-plane simple shear. The version proposed by Camanho and Mayugo [6, 18] combines the Tan and Nuismer solution with the LaRC 04 failure criteria for matrix cracking [14] which are used to predict damage activation and to control damage evolution under multi-axial stress states. The crack density is related to the strain tensor by equating the change of elastic strain energy due to stiffness degradation and the energy dissipated by the creation of a new crack

$$\Delta U/width = 2h_\mathrm{ges} L\, \boldsymbol{\varepsilon} : (\boldsymbol{E}_\mathrm{Lam}(L) - \boldsymbol{E}_\mathrm{Lam}(L/2)) : \boldsymbol{\varepsilon} = 2h_{90}\, G_\mathrm{c,ply} \quad , \tag{6}$$

where $\boldsymbol{E}_\mathrm{Lam}$ is the elasticity tensor of the whole laminate as a function of the crack spacing, $2L$, which is related to crack density, CD, by $2L = 1/CD$. The intra-laminar fracture toughness for a given mode mix, $G_\mathrm{c,ply}$, is determined using the mode-mix criterion proposed by Hahn [21]. The only additional assumption required to obtain the relation between crack density and the strain state is that the multi-axial strain ratio, $\gamma_{xy}/\varepsilon_{xx}$ (x-direction defined as perpendicular to the 90°-ply), remains constant throughout the loading history. The LaRC 04 damage activation functions are computed explicitly by using the same effective stress tensor as defined in Eq. (4) but with $\boldsymbol{\varepsilon}^\mathrm{pl} = \mathbf{0}$ since plasticity is not included in this model, i.e.

$$\boldsymbol{\sigma}^\mathrm{eff} = \boldsymbol{E}^0 : \boldsymbol{\varepsilon} \quad . \tag{7}$$

To account for the non-linear shear response prior to damage onset, the model uses a non-linear elastic relation between in-plane shear stresses and strains (without accounting for any influence of transverse stresses) proposed in [22]

$$\gamma_{12} = \frac{\sigma_{12}}{G_{12}} + \gamma_{12}^\mathrm{NL} = \frac{\sigma_{12}}{G_{12}} + \chi\sigma_{12}^3 \quad , \tag{8}$$

where χ is the shear response factor, a material parameter that is determined from experimental data.

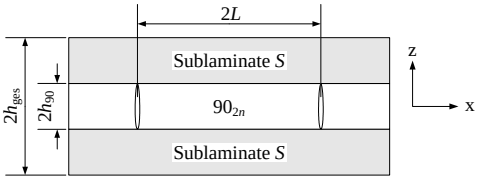

Fig. 2. Periodic cracks in a 90°-ply embedded between orthotropic sub laminates [6, 18].

2.4 Exponential softening model (localized failure)

In contrast to the previous models, the *'ExpSoft'* model proposed by Maimí *et al.* [7, 8] is designed to model localized failure, i.e. the development of a localized crack caused by a stress concentration. It is implemented as a user material for the Finite Element Method (FEM) code `ABAQUS` (Dassault Systèmes Simulia Corp., Providence, RI, USA) and can be used with plane stress (shell) elements and 3D continuum elements. Note however, that only the in-plane stress components are used to assess damage evolution, even if 3D elements are used. The model includes damage due to tensile and compressive failure of both the fibers and the matrix. Here, only degradation due to tensile matrix failure is discussed.

The LaRC 04 failure criteria for transverse matrix cracking [14] are used for predicting damage onset and for controlling the progression of damage based on the effective stress defined in Eq. (7). After damage onset, the shear modulus and transverse Young's modulus are gradually degraded to zero following an exponential softening laws (Fig. 3a). In order to produce results that are independent of element size, the energy dissipated inside an element needs to equal the amount of energy necessary to create exactly one crack through that element. This is achieved by introducing a characteristic length of the element, L_{ch}, following the crack band model by Bažant [23] and computing the energy dissipated per unit volume as

$$\begin{aligned} U_{22}^{\mathrm{dis}} &= \int \sigma_{22} d\varepsilon_{22} = G_{\mathrm{Ic,ply}}/L_{\mathrm{ch}} \\ U_{12}^{\mathrm{dis}} &= \int \sigma_{12} d\gamma_{12} = G_{\mathrm{IIc,ply}}/L_{\mathrm{ch}} \end{aligned} \quad , \tag{9}$$

where $G_{\mathrm{Ic,ply}}$ and $G_{\mathrm{IIc,ply}}$ are the intra-laminar fracture toughnesses for mode I and mode II, respectively. The softening curves for shear and transverse tension are then adjusted such that Eqs. (9) hold. Depending on the chosen element size, it is possible that the energy that needs to be dissipated in the element exceeds the elastic energy at damage onset, i.e. $G_{\mathrm{Ic,ply}}/L_{\mathrm{ch}} < \frac{1}{2} Y^{\mathrm{t}} \varepsilon_{22}^{0}$ or $G_{\mathrm{IIc,ply}}/L_{\mathrm{ch}} < \frac{1}{2} S \gamma_{12}^{0}$, which would lead to "snap-back" in the softening curve of the stress–strain law. Therefore, if the element size is chosen too large, the strengths Y^{t} and S are reduced appropriately in order to avoid this snap-back.

2.5 `ABAQUS` *damage model for composites (localized failure)*

The *'ABQ'* damage model for fiber reinforced composites available in the commercial FEM code `ABAQUS` [9, 24] is in many ways similar to the model

described in Section 2.4. It is also conceived as a localizing damage model that can handle progressive matrix and fiber failure, each modeled differently for tension and compression, and uses Bažant's crack band model [23] to reduce mesh dependency.

In contrast to the *exponential softening* model, however, the `ABAQUS` model uses a linear softening law (Fig. 3b). Furthermore, damage onset is predicted based on the Hashin failure criterion [25] which is applied to an effective stress defined as

$$\hat{\boldsymbol{\sigma}} = \begin{bmatrix} \frac{1}{1-d_\mathrm{f}} & 0 & 0 \\ 0 & \frac{1}{1-d_\mathrm{m}} & 0 \\ 0 & 0 & \frac{1}{1-d_\mathrm{s}} \end{bmatrix} \boldsymbol{\sigma} \quad , \tag{10}$$

where d_f, d_m, and d_s are internal variables controlling the degradation of the in-plane moduli,

$$E_1^\mathrm{d} = (1-d_\mathrm{f})E_1, \quad E_2^\mathrm{d} = (1-d_\mathrm{m})E_2, \quad G_{12}^\mathrm{d} = (1-d_\mathrm{s})G_{12}, \quad . \tag{11}$$

For damage due to tensile matrix failure $d_\mathrm{f} = 0$ and $d_\mathrm{s} = d_\mathrm{m}$, i.e. E_2^d and G_{12}^d follow the same degradation law. Degradation is controlled by an equivalent displacement, δ_eq, which takes the characteristic length into account such that the softening curve from damage onset to ultimate failure is linear (Fig. 3b) and the energy dissipated by the damage process corresponds to the energy required to create one crack inside an element

$$U^\mathrm{dis} L_\mathrm{ch} = \tfrac{1}{2}\, \sigma_\mathrm{eq}^0 \delta_\mathrm{eq}^\mathrm{f} = G_\mathrm{Ic,ply} \quad , \tag{12}$$

where the equivalent stress at damage onset, σ_eq^0, is a function of the in-plane shear and transverse normal stresses and strains. Snap-back is not allowed in this model, i.e. $\delta_\mathrm{eq}^f \geq \delta_\mathrm{eq}^0$ always holds true. However, in this model the strengths are not adjusted. If the chosen element size is too large, the energy dissipated in the element is greater than $G_\mathrm{Ic,ply}/L_\mathrm{ch}$.

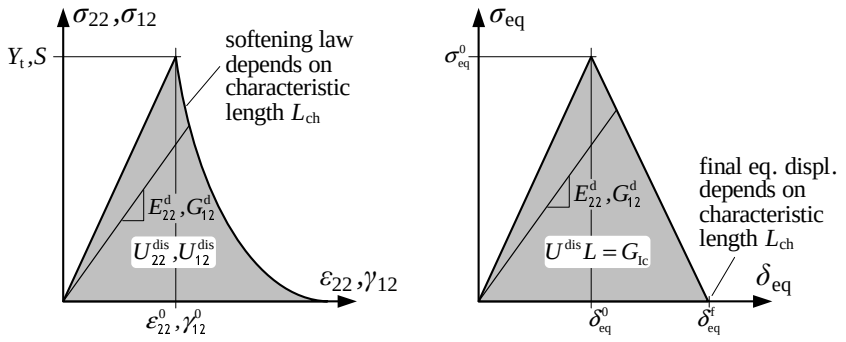

(a) (b)

Fig. 3. Softening laws for localized damage models using Bazant's crack band model; (a) *exponential softening* model [7, 8]; (b) `ABAQUS` damage model [9, 24].

Table 1
Material constants of the glass fiber/epoxy material [27, 28, 29] used in the analyses.

Elastic properties				toughnesses		slope parameter
E_1	E_2	G_{12}	ν_{12}	$G_{\mathrm{Ic,ply}}$	$G_{\mathrm{IIc,ply}}$	$p^{\mathrm{t}}_{12} = \eta_{\mathrm{L}}$
[GPa]	[GPa]	[GPa]		[kJ/m^2]	[kJ/m^2]	
44.73	12.8	5.8	0.3	0.4	0.8	0.3

3 MATERIAL PROPERTIES AND PARAMETERS USED IN THE ANALYSES

All model predictions that are presented in this work are computed using the same set of material data which corresponds to the glass fiber / epoxy material used in the experiments described in Section 5. The material data used in the analyses is summarized in Table 1. In addition to the elastic properties, intra-laminar toughnesses and a slope parameter are required. The toughnesses $G_{\mathrm{Ic,ply}}$ and $G_{\mathrm{IIc,ply}}$ are used to compute in-situ strengths (see Section 3.2). The slope parameter, $p^{\mathrm{t}}_{12} = \eta_{\mathrm{L}}$, determines the slope of the damage activation functions for the *Mori-Tanaka* model and the *constant stress* model in $\sigma_{22}-\sigma_{12}$ stress space at $\sigma_{22} = 0$, and is chosen as suggested by Puck *et al.* [26] as $p^{\mathrm{t}}_{12} = \eta_{\mathrm{L}} = 0.3$.

The damage part of the *Mori-Tanaka* model requires two additional parameters: the aspect ratio of the Mori-Tanaka inclusions, which is chosen as $e_{\mathsf{n}} = 0.001$ to resemble the crack-like geometry, and the damage evolution parameter, which is set to $\kappa = 0.05$ such that damage onset occurs 5% below the nominal failure load at $FI = 0.95$. Note that for $\kappa = 0$, damage onset would occur at $FI = 1$ and the failure index would stay constant during damage progression. Hence, for uni-axial transverse tension, the *Mori-Tanaka* model would give the same response as the *constant stress* model.

3.1 Plasticity response

The non-linear shear response of the chosen glass/epoxy material has been characterized in Ref. [28] by determining the change of secant shear modulus with shear strain based on tensile tests of $(\pm 40)_{\mathrm{s}}$ and $(\pm 27)_{\mathrm{s}}$ laminates. The experimental data shown in Fig. 4b is derived from measurements of laminate's axial modulus, E_{xx}, and Poisson's ratio, ν_{xy}. The results of these tests are used to calibrate the plasticity response of the *Mori-Tanaka* model, the *constant stress* model, and the *periodic crack* model. The relation between shear stress and plastic shear strain (Fig. 4a) can be derived from the original data by using the initial shear modulus and factoring out the elastic shear strain.

For the *periodic crack* model, the non-linear shear strain is approximated by the function in Eq. (8) with $\chi = 2 \times 10^{-8}\,\mathrm{MPa}^{-3}$ [6]. For the *Mori-Tanaka* model, the plastic shear strain is approximated by the analytical curve fit

$$\gamma_{12}^{\mathrm{pl}} = \left(\frac{\sigma_{12}}{k}\right)^{n} \quad \text{with} \quad n = 7,\ k = 147\,\mathrm{MPa} \quad . \tag{13}$$

Note that Eq. (13) would be equivalent to the non-linear part of Eq. (8) for $n = 3$. However, it has been found that a higher exponent typically yields a better description of the non-linear shear response for composites with epoxy or PEEK matrix [10].

The plasticity law for the *constant stress* model is formulated in terms of the normalized secant shear modulus change vs. equivalent shear strain (Fig. 4b). Both a linear and a non-linear curve fit are used to define f_{12} in Eq. (3) as

$$\begin{aligned} f_{12} &= -28\,\varepsilon_{\mathrm{eq}} + 1.19 && \ldots \text{linear fit} \\ f_{12} &= 469\,(\varepsilon_{\mathrm{eq}})^2 - 38\,\varepsilon_{\mathrm{eq}} + 1.22 && \ldots \text{non-linear fit} \quad . \end{aligned} \tag{14}$$

Due to the lack of experimental data for the plastic transverse response, the same function is used in the transverse direction, i.e. $f_2 = f_{12}$. Based on the non-linear data for a glass fiber / epoxy material in another study [30], this seems to be a reasonable assumption. Nevertheless, this estimation has to be kept in mind for predictions that involve plasticity under transverse tension.

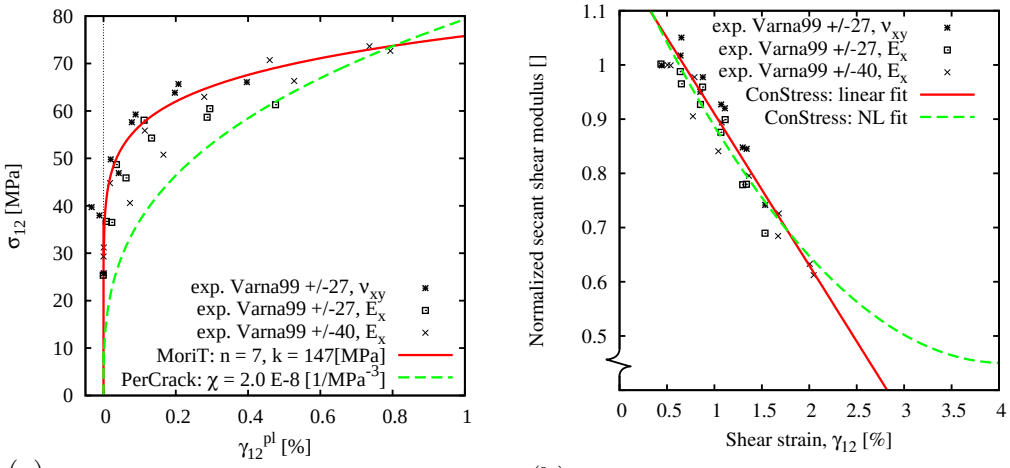

Fig. 4. Analytical curve fits for non-linear shear response derived from experimental data given in Ref. [28]; (a) *Mori-Tanaka* and *periodic crack* model, σ_{12} vs. $\gamma_{12}^{\mathrm{pl}}$; (b) *constant stress* model, $G_{12}\,\mathrm{sec}\,/G_{12}^{0}$ vs. γ_{12}.

Table 2
In-situ strengths used in analyses for 4-ply and 8-ply laminates (values in MPa).

	$Y^{\mathrm{t}}_{\mathrm{linear}}$	$Y^{\mathrm{t}}_{\mathrm{non\text{-}linear}}$	S
8-ply strength	76	72	73
4-ply strength	107	93	82

3.2 In-situ strength

Experimental data shows that matrix cracking in an embedded ply occurs at higher stresses than in a single ply or UD-laminate (e.g. [31, 32, 33, 34]). Assuming that matrix cracks are caused by propagation of pre-existing flaws, this 'in-situ' effect can be explained by the initial flaw size being limited to the ply thickness, and the presence of neighboring plies which changes the boundary conditions of the underlying fracture mechanics problem. Camanho *et al.* [22] proposed to account for the in-situ effect by introducing in-situ strengths that depend on ply thickness. The in-situ strengths are derived based on fracture mechanics by comparing the energy released by crack formation to the material's intralaminar fracture toughness. The energy released in the embedded ply during crack formation depends on the ply's constitutive law. Therefore, any non-linearity prior to damage onset needs to be accounted for in the computation of in-situ strengths.

Two types of laminates are considered in the current study; laminate A with a 12-ply $(\pm\beta/90_4)_{\mathrm{s}}$ layup and laminate B with a 19-ply $(0/\pm\beta_4/0_{1/2})_{\mathrm{s}}$ layup, where the 1/2 subscript indicates a half ply. Damage in these laminates occurs primarily in the 8-ply stack of 90°-layers of laminate A and in the angle-plies of laminate B with a thickness of four plies for $+\beta$ and $-\beta$, respectively. It has been found in a previous study [10], that in-situ strengths need to be used for these layers to obtain good correlation with experimental data. However, it is not possible to assign individual in-situ strengths for each ply in the currently implemented versions of some of the models. Therefore, the same in-situ strengths are used for all plies of one laminate in order to produce comparable results, i.e. all plies in laminate A are assigned 8-ply in-situ strengths while the plies in laminate B have 4-ply in-situ strengths (see Table 2). The effect of different in-situ strengths has been studied in detail in [10].

For transverse tension, all models except the *constant stress* model assume a linear response and the corresponding in-situ strength $Y^{\mathrm{t}}_{\mathrm{linear}}$ is computed as proposed by Camanho *et al.* [22] from the intralaminar Mode I fracture toughness, $G_{\mathrm{Ic,ply}}$. An in-situ transverse strength for non-linear transverse behavior, $Y^{\mathrm{t}}_{\mathrm{non\text{-}linear}}$, is used for the *constant stress* model following a modification of Camanho's approach by Pinho *et al.* [12].

Table 3
Non-standard input parameters required by the damage models for predicting transverse matrix cracking (values indicated by $^{*)}$ are derived from experimental data).

model	plasticity	damage initiation	damage evolution
Mori-Tanaka	$n^{*)}, k^{*)}$	p_{12}^{t}	e_{n}, κ
constant stress	$f_{12}{}^{*)}, f_2$	η_{L}	N/A
periodic crack	$\chi^{*)}$	η_{L}	N/A
exp. softening	N/A	η_{L}	N/A
`ABAQUS`	N/A	N/A	N/A

The in-situ shear strength is computed from the mode II fracture toughness, $G_{\mathrm{IIc,ply}}$, for the non-linear shear formulations of the *Mori-Tanaka*, the *constant stress*, and the *periodic crack* models and yields the same value for all three models. The *exponential softening* model and the `ABAQUS` model use a linear shear response. The in-situ shear strength for a linear shear response would amount to 101 MPa and 143 MPa for 8-ply and 4-ply stacks, respectively. These values are unrealistically high considering the maximum attainable shear stress shown in Fig. 4a. Therefore, the in-situ shear strength for non-linear shear is used for the last two models as well. Note, however, that this inaccuracy has little effect on the predictions presented in the following for the *exponential softening* model and the `ABAQUS` model since those two models are only applied to test cases where damage is dominated by transverse tension.

3.3 Parameter identification

Most of the damage models discussed in this work require some input parameters that are not readily available from standard test methods. The parameters required by each of the models in addition to ply stiffnesses, strengths and intra-laminar toughnesses are listed in Table 3. Except for the empirical plasticity parameters for in-plane shear (marked by $^{*)}$), all of the parameters in Table 3 had to be estimated for the glass fiber material considered here. This seems to be a drawback of these models. However, some bounds for an appropriate choice of the lacking parameters can be given.

Plasticity under transverse tension has not yet received much attention in the literature. But from a theoretical point of view it is reasonable to set $f_2 = f_{12}$ since plasticity under transverse tension is caused by the same mechanism as shear plasticity.

Values for slope parameters, p_{12}^{t} or η_{L}, of typical glass and carbon fiber materials can be found in the literature [13, 26] and are consistently in a range of

0.25 - 0.35. Note that the slope parameters can also be set to zero, in which case the Puck and LaRC 04 failure criteria would yield the same result as the simpler Hashin criterion used by the ABAQUS model.

The *Mori-Tanaka* model offers two parameters for adjusting the degradation behavior. The aspect ratio, e_n, has to be chosen very small to resemble the crack-like geometry. However, reducing the aspect ratio to values smaller than 0.001 hardly changes the predicted degradation further [35]. The evolution parameter, κ, accounts for the statistical variation in the local strength of a ply and can therefore be estimated based on the scatter of experimental data. Choosing $\kappa = 0$ corresponds to zero strength variation and predicts the stress to remain constant after damage onset, similarly to the *constant stress* model.

4 QUALITATIVE COMPARISON OF DAMAGE MODELS

In this section, the five models are compared qualitatively. The comparison emphasizes the differences between the model formulations and implications of the modeling assumptions.

4.1 Plasticity

Some recent experimental investigations have shown that laminates subjected to loads that mainly lead to ply shear stresses exhibit a significant amount of residual strains after unloading [36, 37]. Figure 5a shows experimental data of a uniaxial tension test on a symmetric ±45 laminate including several loading cycles [37]. The loops reveal that the non-linearity caused by the shear stresses is initially related to residual strains while the shear modulus (indicated by

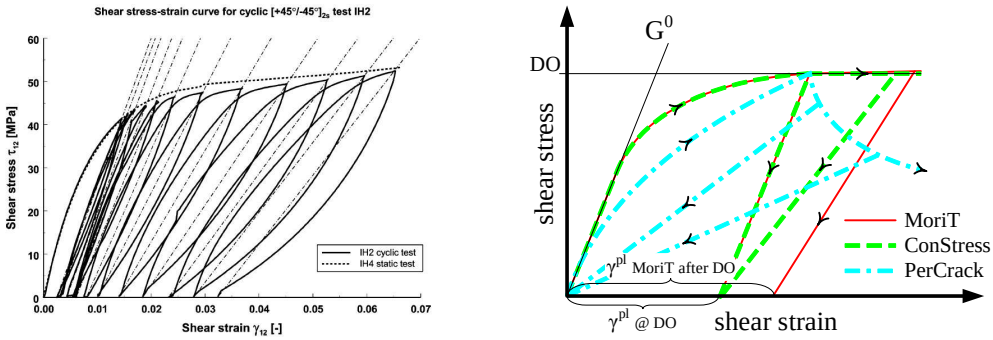

(a) (b)

Fig. 5. (a) Non-linear shear stress–shear strain response of a symmetric ±45 laminate under uniaxial tension; (experimental results [37]); (b) schematic of model predictions (DO = damage onset).

dashed lines) remains approximately constant at first. At higher loads, the shear modulus starts to change significantly accompanied by a further accumulation of residual strain. Note that the hysteresis loops also found in the experiments, which could be the result of viscous effects, are not considered by any of the models.

The *Mori-Tanaka* and the *constant stress* models account for residual strains using plasticity formulations. A schematic of the shear response predicted by those two models is shown in Fig. 5b as red solid and green dashed lines, respectively. Both models assume that the non-linearity prior to damage onset (DO) is caused by plasticity only. Therefore, any unloading curves below damage onset follow the initial slope of G^0. After damage onset, the *constant stress* model assumes no further accumulation of plastic strain, i.e. all non-linearity after damage onset is caused by matrix damage. In the *Mori-Tanaka* model, the plastic strain is a function of shear stress and since the stress continues to increase slightly after damage onset, the amount of plastic strain continues to grow in this model. Note that for $\kappa = 0$, the failure index in the *Mori-Tanaka* model would remain constant during damage progression, which means that the stresses and the plastic strain would not increase after damage onset (for a constant ratio of shear vs. transverse stress).

Also shown in Fig. 5b is a schematic of the response from the *periodic crack* model, which accounts for shear non-linearity by a non-linear elastic stress–strain law. Therefore, the same non-linear curve is followed for loading and unloading as long as the maximum stress does not exceed the damage onset stress. After damage onset, the stresses decrease with increasing load and the unloading path would be linear and leading back to the origin.

When only monotonic loading (in each material point) is considered, the definition of the unloading path is without consequence. For non-monotonic loading, which can occur locally due to damage even if the global load is applied monotonically, using the correct unloading path is important for predicting the redistribution of stresses accurately.

4.2 Distributed vs. localized cracking

If a ply embedded in a laminate is subjected to a homogeneous stress or strain field, the first matrix crack that spans the whole thickness of a ply typically does not lead to laminate failure since stresses can locally be transferred to adjacent layers. Consequently, an array of matrix cracks will develop and accumulate more or less evenly throughout the ply (left side of Fig. 6).

The response of a ply containing an array of cracks can be modeled by continuum mechanics provided that the size of the volume considered is large com-

pared to the width of a crack (homogenization requirement). The stresses given by a continuum model should equal the volume average of the actual stresses ('stress distribution' in Fig. 6). As the number of ply cracks increases with load, the volume averaged stresses may decrease but as long as the ply interfaces and the adjacent plies are intact, they remain non-zero due to the stresses transferred through the ply interfaces ('stress–strain response' in Fig. 6). At some point, the increase of crack density with load will saturate since the stress transfer is limited by the strength of the ply interfaces. The first three models presented in Section 2 are intended to model this behavior up to crack saturation, with damage progression corresponding to the increasing number of ply cracks. Note that delamination after crack saturation can be handled by the *constant stress* model but is not considered in the present study.

The last two models of Section 2 (*ExpSoft* and *ABQ*) are intended for modeling localized damage, i.e. the response due to a single crack. In those models, the progression of damage has to be interpreted as the formation of micro-cracks and their ultimate coalescence into a ply crack (Fig. 7). For a single ply, it is clear that in such a model the stresses have to be reduced to zero in the ultimate damage state where the material has been completely separated. For a ply embedded in a laminate, ply stresses will be zero at the crack but not further away from it as long as the ply interfaces are intact. Consequently, the assumption inherent to the localized damage models that shear and transverse stresses become zero when the ply crack has fully formed are only valid if homogenization is performed over a volume approximately the size of the cracked domain (`vol.1` in Fig. 7). The element size in an FEM computation, however, will typically be much larger than this for reasons of numerical efficiency (for example, similar to `vol.2` in Fig. 7). The stresses averaged over `vol.2` do not

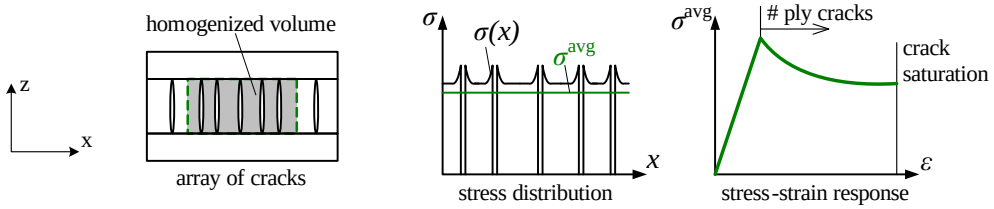

Fig. 6. Homogenization volume, stresses distribution, and stress–strain response for distributed cracking.

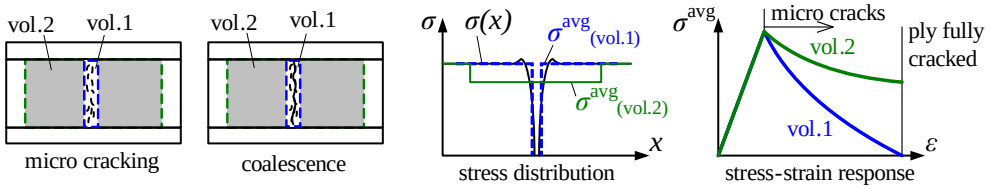

Fig. 7. Homogenization volumes, stresses distributions, and stress–strain responses for localized cracking.

tend to zero since a considerable part of the volume is undamaged and loaded through shear stresses along the ply interfaces. From these considerations it is obvious that the two models for localized damage will not give very accurate predictions for homogeneous loading since the ply interfaces are expected to stay intact until crack saturation. Laminates subjected to inhomogeneous stress fields (e.g. near a notch) often develop one dominant 'splitting' crack accompanied by local delamination (e.g. [38]), in which case stresses vanish in a larger area around the crack.

The present review focuses on damage due to matrix cracking under homogeneous stress / strain states prior to crack saturation from loads that lead to an array of matrix cracks but leave the interface intact. As detailed above, the localizing damage models are not intended for this purpose. However, they will be included in the present comparison in order to point out and discuss the effects of different implementation strategies. Analyses using the localized damage models (*ExpSoft* and *ABQ*) are performed by applying the homogeneous load to a single, 4-noded finite element. Since the laminate response predicted by the localized damage models is not fixed, but depends on the characteristic element length, the element size is chosen as the distance between two cracks at crack saturation, $2L^{\mathrm{sat}}$, which is estimated by the following approach.

Crack saturation occurs when the distance between two cracks is so small that the ply stresses, transmitted via the interface from neighboring plies, do not exceed the tensile failure stress. The stresses transmitted through the interface are limited by the interface shear strength. Based on a shear lag model for an embedded ply under uniaxial transverse tension (Fig. 8a) and assuming the shear stress along the ply interface to be constant and equal to the interface shear strength, S^{IF}, the crack spacing at saturation can be estimated as

$$2L^{\mathrm{sat}} = t\,Y^{\mathrm{t}}/S^{\mathrm{IF}} \quad , \tag{15}$$

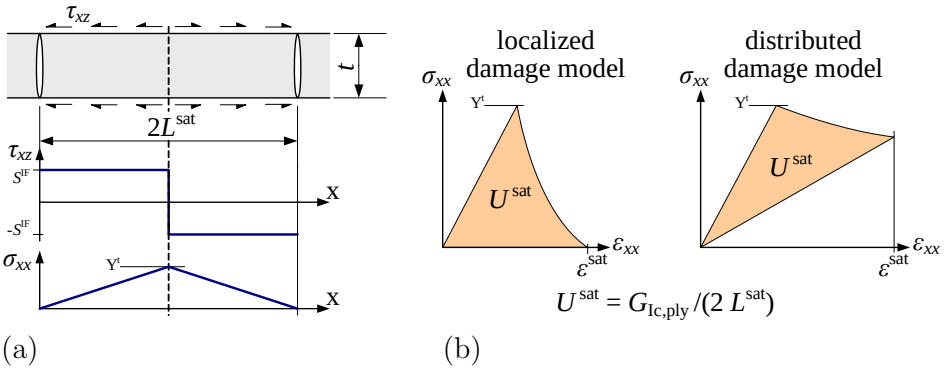

(a) (b)

Fig. 8. (a) Shear lag model used to estimate the crack spacing at crack saturation, (b) schematic of stress–strain response and dissipated energy density at crack saturation.

where t denotes the thickness of the cracked ply (or cluster of like oriented plies). Based on the linear in-situ strengths for transverse tension (Table 2) and estimating the interlaminar shear strength as $S^{\mathrm{IF}} = 73\,\mathrm{MPa}$, the crack spacing is computed from Eq. (15) as $2L^{\mathrm{sat}} = 1.2\,\mathrm{mm}$ and $2L^{\mathrm{sat}} = 0.84\,\mathrm{mm}$ for the laminates with 8-ply and 4-ply in-situ strengths, respectively. The dissipated energy density predicted by the localized damage models then amounts to $U^{\mathrm{sat}} = G_{\mathrm{Ic,ply}}/(2L^{\mathrm{sat}})$, which equals the energy density dissipated by the distributed damage models up to the saturation stage (see Fig. 8b).

The stress–strain response for an embedded ply under transverse tension is shown in Fig. 9a. The experimental results are derived from data provided in [29], Varna01, and [28], Varna99, for uniaxial tension tests on flat specimens with a $(0_2/90_4)_{\mathrm{s}}$ and a $(0/90_8/0_{1/2})_{\mathrm{s}}$ lay-up, respectively, by assuming that the change in the laminate response is only the result of a change in the transverse Young's modulus of the 90-ply clusters. Note that a change of G_{12} is irrelevant to the response of a 0/90-laminate under uniaxial tension.

As can be expected, Fig. 9a shows that the prediction of the *periodic crack* model is the most accurate since that model is an exact solution of the corresponding boundary value problem. The two localized damage models *ExpSoft* and *ABQ* predict the stresses to reduce to zero which does not agree with the experimental data due to the reasons discussed above. The *Mori-Tanaka* model predicts ply stresses to be almost constant after damage onset, which is a result of the damage evolution law chosen. The response of the *constant stress* model is very similar, but with a small amount of non-linearity prior to damage onset, due to the plasticity law for transverse tension, and with the stress remaining constant after damage onset as imposed by the model's assumption. Note that according to Joffe *et al.* [27], no cracks were observed in the $(0_2/90_4)_{\mathrm{s}}$ laminate below a strain of $\varepsilon_{xx} \approx 0.6\%$ ($\varepsilon_{xx} = \varepsilon_{22}$ in Fig. 9).

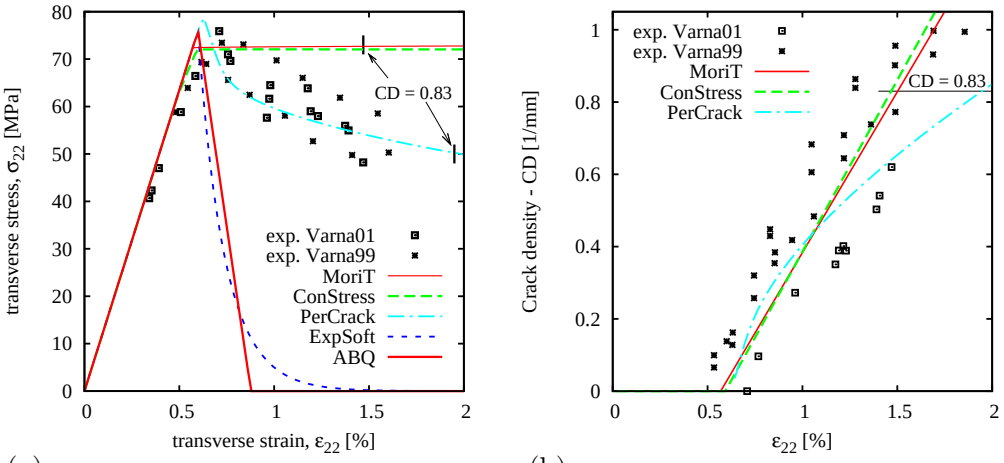

Fig. 9. Embedded 90°-ply in 0/90 lay-up under uniaxial tension: (a) stress strain response, (b) accumulation of matrix cracks; experimental data from [28, 29].

However, the experimental data shows some small non-linearity starting at slightly lower strain. This could be an indication that plasticity indeed occurs in the 90° ply prior to damage onset, as assumed in the *constant stress* model.

Figure 9b shows the increase of crack density, CD, as a function of axial strain for the same two cross-ply laminates. In the *periodic crack* model, crack density is an internal variable and is therefore directly available for plotting. Note however, that the *periodic crack* model is strictly only valid for the $(0_2/90_4)_s$ laminate (corresponding to data points labeled exp. Varna01 [29]) and not to the other lay-up. The crack densities for the *Mori-Tanaka* and *constant stress* models are computed by dividing the predicted energy density dissipated due to damage, U^{dis}, with the energy dissipated by the formation of one crack, $G_{\text{Ic,ply}}$, i.e. $CD = U^{\text{dis}}/G_{\text{Ic,ply}}$. The predictions of these two models are the same for both laminates (solid red and dashed green lines, respectively, in Fig. 9b).

Also indicated in Fig. 9 is the strain at which the saturation crack density, $CD^{\text{sat}} = 1/(2L^{\text{sat}}) = 0.83/\text{mm}$, based on the shear lag model for the $(0_2/90_4)_s$ laminate, is reached. This saturation crack density strain is $\varepsilon_{xx} \approx 1.5\%$ for the *Mori Tanaka* and the *constant stress* models, and $\varepsilon_{xx} \approx 1.95\%$ for the *periodic crack* model. As noted above, the energy dissipation per unit volume predicted by these three models for $CD = 0.83/\text{mm}$ is the same as the energy density dissipated by the localized damage models for this lay-up.

4.3 Damage activation and damage evolution

The damage models considered in this study use stress based failure envelopes to predict damage onset. These failure criteria distinguish between matrix and fiber failure for both tension and compression, and accordingly, use separate functions for each failure mode. For tensile matrix failure in plane stress, which is investigated here, only in-plane shear and transverse tensile stresses are relevant. The failure envelopes for matrix tension can thus be plotted in σ_{12}–σ_{22} stress space (see Fig. 10) and show only minor differences between the failure criteria. The main difference is the slope of the failure envelope at $\sigma_{22} = 0$. The Hashin criterion assumes zero slope at that point, while the Puck 2D and the Mohr-Coulomb based criteria require an additional material parameter to determine the slope, and the LaRC 04 criterion determines the slope by the ply's strengths and toughnesses (see Section 3). Note that the envelopes in Fig. 10 are plotted for 8-ply in-situ strengths. The in-situ strength for transverse tension used by the *constant stress* model takes plasticity into account and is therefore lower than for the other models (cf. Table 2).

With respect to the damage activation functions, it should be noted that the Hashin and Puck 2D equations only contain stress components to the power of one. Therefore, as long as the material response is linear, the failure index given by Hashin and Puck 2D scales linearly with load, and the failure load is given by $\boldsymbol{\sigma}^0 = \boldsymbol{\sigma}/FI$. The failure index computed using the LaRC 04 and the Mohr-Coulomb criteria cannot be interpreted this way since the corresponding equations contain first and second order terms of σ_{22}. The advantages of a linear failure index, however, are only relevant for linear analyses (e.g. 'First Ply Failure' analysis). In a damage analysis, the failure index generally does not scale with load since the material response is non-linear.

As long as a ply is undamaged, the application of stress based damage activation functions is straight forward. Once a ply has been damaged, the correct stresses to use for evaluating the damage activation functions need to be identified. Perhaps the most intuitive solution is to use the homogenized ply stresses given by the constitutive model as proposed by the *Mori-Tanaka* model. The disadvantage of this approach is that the constitutive equation of the damage model needs to be solved iteratively, since the stress state depends on the damage state, and vice versa.

One way to obviate the need for iteration is to introduce an effective stress tensor that is independent of the damage state (Eqs. (4) and (7) for models *ConStress*, *PerCrack*, and *ExpSoft*). The drawback with this method is that it does not account for the changing stress–strain coupling in the longitudinal and transverse directions that is caused by damage. Hence, the damage prediction of secondary failure modes may be inaccurate. Consider, for example, a uni-directional laminate under transverse tension that has been damaged due to matrix cracking. Because of the damage, the minor Poisson's ratio, ν_{21},

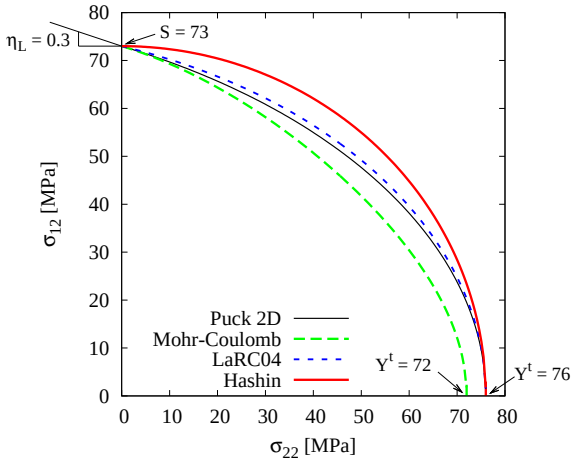

Fig. 10. Damage activation functions for tensile matrix failure used by the damage models: Puck 2D for *MoriT*, Mohr-Coulomb for *ConStress*, LaRC 04 for *PerCrack* and *ExpSoft*, and Hashin for *ABQ*.

approaches zero and the contraction in fiber direction vanishes. The effective stress is defined as the stress state that would exist if an undamaged ply were subjected to the same strain state (i.e. $\varepsilon_{22} > 0$, $\varepsilon_{11} \approx 0$). Since the minor Poisson's ratio of an intact ply is larger than in a damaged ply, this strain state results in a non-zero effective stress in the fiber direction, $\sigma_{11}^{\text{eff}} > 0$. In the worst case, depending on the material properties and the degradation laws used, this effective stress can result in a predicted fiber failure even though the ply is only loaded in the transverse direction.

The `ABAQUS` damage model also uses an effective stress tensor to predict damage initiation. However, this tensor is defined by scaling the components of the homogenized stress tensor individually based on the corresponding damage variable, d_{f}, d_{m}, or d_{s}, (see Eq. 10) which circumvents the problem above. The effective stress tensor used by the `ABAQUS` damage model depends on the damage state (defined by the damage variables). Nevertheless, there is no need for iteration because once damage has initiated, the evolution of the damage state in this model is a function of the strain state only. The drawback of using strains to control damage evolution, however, is that due to the ply coupling constraints in laminates, stresses and strains do not necessarily correlate. Damage progression observed experimentally is typically driven by stresses rather than strains. For example, uniaxial tension of a 0/90 laminate first causes matrix cracking in the 90°-plies, but with increasing load, cracks develop also in the 0°-plies. This is a result of the constraint of the Poisson effect imposed by the 90°-layers that leads to transverse tensile stresses in the 0°-plies. If this loading scenario is analyzed using the `ABAQUS` damage model, the Hashin criterion correctly predicts damage initiation due to matrix tension in the 0°-plies. However, there is no damage evolution in those plies because the transverse strain, ε_{22}, is negative, indicating compression. Consequently, the equivalent displacement for matrix tension, which controls damage evolution for this failure mode, is zero and the development of cracks in the 0°-plies cannot be captured.

4.4 Stiffness degradation and anisotropy of damage

The effect of matrix cracks on the homogenized ply stiffnesses varies in different directions because of the crack geometry. A damage model for matrix cracking thus needs to capture this anisotropy of damage by degrading the various components of the elasticity tensor differently. For orthotropic materials under plane stress, the material response is determined by four independent variables E_1, E_2, G_{12}, and ν_{12}. Figure 11 shows the change of those four material parameters, normalized by their respective initial values, as predicted by the five damage models for a $(0_2/90_4)_{\text{s}}$ laminate under uniaxial tension.

In the *Mori-Tanaka* model (Fig. 11a), the different degradation of the properties is a result of the chosen aspect ratio of the Mori-Tanaka inclusions. An aspect ratio of $e_{\mathsf{n}} = 1$ would lead the degradation of all properties to be equal (isotropic damage). To mimic the effect of thin cracks, the aspect ratio has to be chosen very small (e.g. $e_{\mathsf{n}} = 0.001$) which results in a barely noticeable increase of E_1 and ν_{12}, and a degradation for E_2 that is different than the degradation for G_{12}. Note that all other models assume E_1 and ν_{12} to remain constant, which leads to a degradation of the minor Poisson's ratio which is equal to that of the transverse Young's modulus, $\nu_{21}/\nu_{21}^0 = E_2/E_2^0$. The same result would be obtained with the *Mori-Tanaka* model for perfectly thin cracks (i.e. $e_{\mathsf{n}} \to 0$).

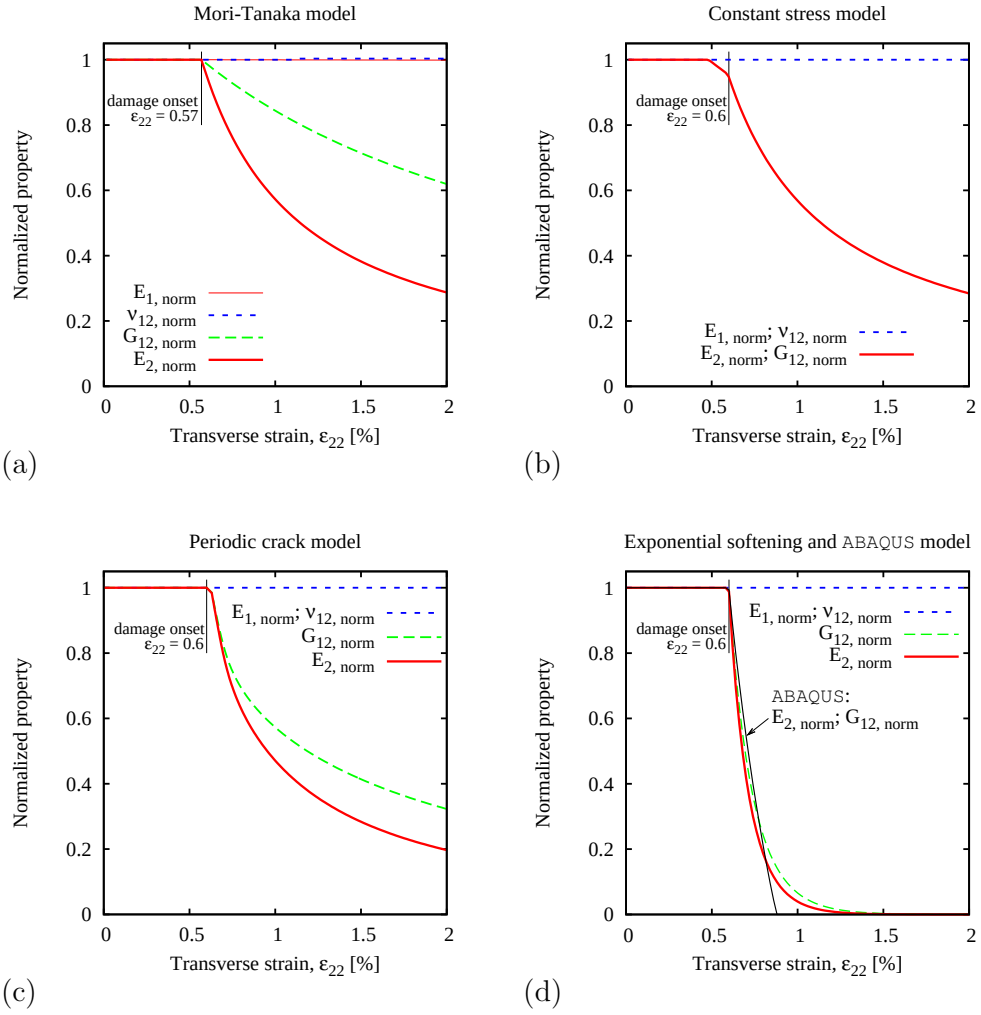

Fig. 11. Predicted degradation of elastic properties: (a) *Mori-Tanaka* model; (b) *constant stress* model; (c) *periodic crack* model; (d) *exponential softening* model and `ABAQUS` model.

In the *periodic crack* model (Fig. 11c), the degradation of E_2 and G_{12} comes from the solution of the boundary value problem of a unit cell containing one crack. Note that both the *Mori-Tanaka* and the *periodic crack* models predict a greater degradation in the transverse Young's modulus than in the shear modulus. This observation generally holds true for other material systems as well (glass and carbon fiber / epoxy composites).

For the *constant stress* model (Fig. 11b), the degradation of E_2 is chosen such that the ply stress remains constant after damage onset. Therefore, the E_2-degradation of the *constant stress* model is very similar to that of the *Mori-Tanaka* model, which also predicts an almost constant ply stress, and slightly less than that of the *periodic crack* model, which shows a softening behavior (Fig. 9). The degradation of G_{12} in the *constant stress* model is assumed to equal that of E_2. Note that for the *constant stress* model, the transverse tensile stresses in the 90°-ply lead to plasticity prior to damage onset, causing the linear degradation between $\varepsilon_{22} \approx 0.5$ and $\varepsilon_{22} = 0.6$. The curves plotted for the *constant stress* model thus represent the changes of secant moduli rather than those of elastic moduli. As a result of the assumption $f_{12} = f_{22}$ for the given material (Sec. 3), the effect of plasticity in the *constant stress* model here is the same for E_2 and G_{12}, however, this is not generally the case.

In the localized damage models, *exponential softening* and `ABAQUS` (Fig. 11d), the degradations of E_2 and G_{12} are determined by the degradation functions for shear and transverse tension and depend on element size. In general, those two models predict a much faster degradation of E_2 and G_{12} than the first three models since they assume the stresses to reach zero in the fully damaged state (i.e. $E_2 = G_{12} = 0$). The degradation of G_{12} in the `ABAQUS` model equals the degradation of E_2 (solid black line in Fig. 11d). In the *exponential softening* model, the degradation of E_2 and G_{12} are computed separately as functions of the respective strength and fracture toughness for transverse tension and shear, as well as the characteristic element length. In some cases, this can lead to the shear degradation exceeding the transverse degradation. However, in the ultimate damage state, the degradation of the two moduli is the same since both are degraded to zero.

5 COMPARISON TO EXPERIMENTAL DATA

For a quantitative assessment of the five models, predictions are evaluated against experimental data from two series of uni-axial tension tests conducted by Varna *et al.* [28, 29]. For each test, the degradation of the laminate's axial modulus and Poisson's ratio are compared. The parameters for the glass fiber / epoxy material used are listed in Table 1. Residual thermal stresses are not taken into account in the present study. The effect of curing stresses for

the same set of experimental tests has been studied in [10] using the *Mori-Tanaka* damage model and was found to be small compared to the scatter of data.

Since the stress / strain state in the specimens is homogeneous, the loading leads to a series of matrix cracks spread uniformly throughout the whole specimen. The increasing crack density was also recorded during the experiments [28, 29]. The localized damage models from Sections 2.4 and 2.5 are not intended for modeling progressive cracking under homogeneous loading and their predictions cannot be expected to correlate well with the experimental data. Nevertheless, these two models are included in the comparison as well in order to gain an understanding of how big the deviation is.

5.1 Laminates type A: embedded 90° plies $(\pm\beta/90_4)_s$ [27, 29]

The laminates type A have a lay-up of $(\pm\beta/90_4)_s$ with four different lay-up angles $\beta = 0°, 15°, 30°, 40°$. The predictions of analyses compared to experimental data [29] are shown in Figs. 12–15. Damage in these laminates is dominated by matrix cracking in the 90° plies and crack density was monitored in these layers only during the experiments. However, all damage models (except for the *periodic crack* model which assumes cracking to occur only in the 90° layer) also predict damage in the angle-plies. The load at which the models predict the onset of cracking in the angle-plies depends on the angle β and on the chosen in-situ strengths. Here, 8-ply in-situ strengths (Table 2) are used for all plies. The effect on the predicted load response of using different in-situ strengths for each ply depending on the ply's thickness and location is addressed in a previous study based on the *Mori-Tanaka* damage model [10].

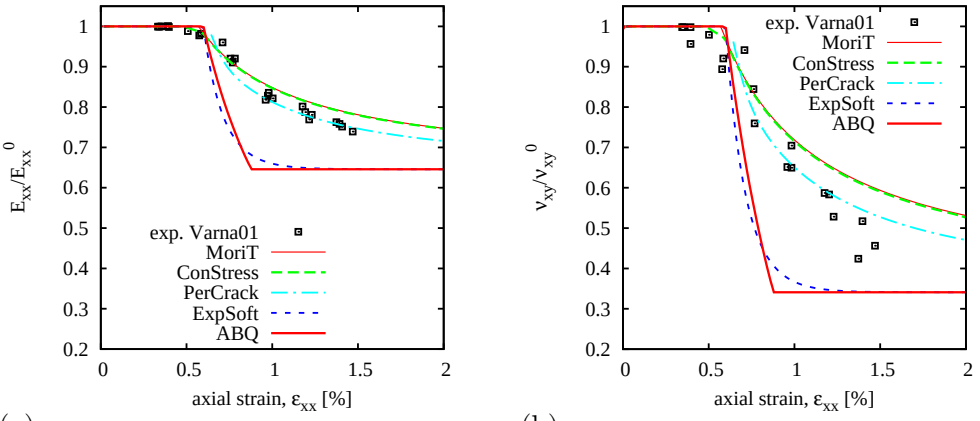

Fig. 12. Results for lay-up $(0_2/90_4)_s$; (a) laminate's axial modulus and (b) Poisson's ratio, normalized by their initial value; experimental data from [29].

The figures show that, in general, predictions from the three distributed damage models are fairly similar, especially as long as cracking only occurs in the 90° plies, and that the correlation with experiments is quite good. The *periodic crack* model predicts slightly more degradation of laminate axial stiffness than the *Mori-Tanaka* and the *constant stress* models (Figs. 12a–15a) and the *periodic crack* predictions correlate very well with the test data for $\beta = 0°$ and $\beta = 15°$. For $\beta = 30°$ and $\beta = 40°$, damage in the angle plies leads to additional degradation of the laminate axial stiffness which is disregarded by the *periodic crack* model. As a result, predictions of the *Mori-Tanaka* and *constant stress* models are slightly better than the *periodic crack* model for those two lay-ups once cracking starts in the angle plies.

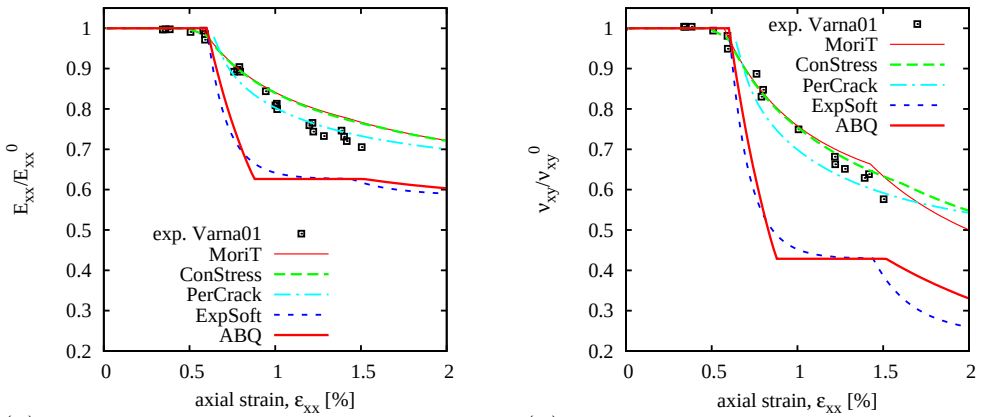

Fig. 13. Results for lay-up $(\pm 15/90_4)_s$; (a) laminate's axial modulus and (b) Poisson's ratio, normalized by their initial value; experimental data from [29].

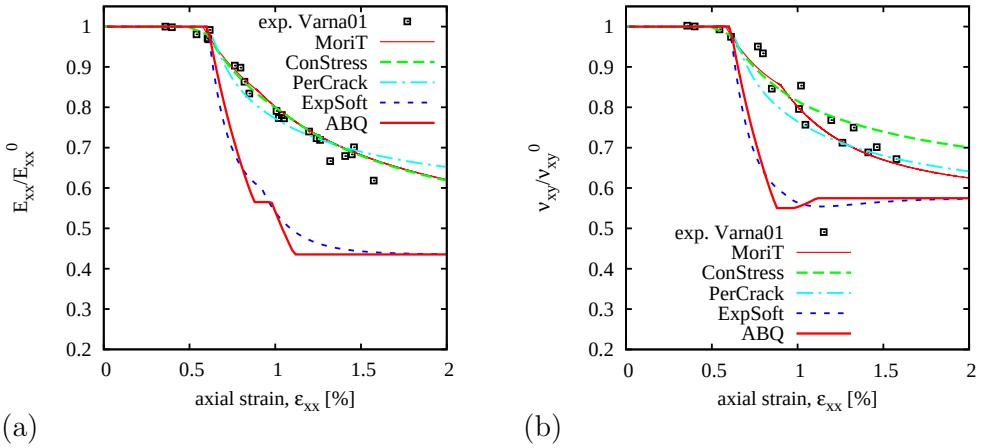

Fig. 14. Results for lay-up $(\pm 30/90_4)_s$; (a) laminate's axial modulus and (b) Poisson's ratio, normalized by their initial value; experimental data from [29].

Similar observations can be made regarding the degradation of laminate Poisson's ratio (Figs. 12b–15b). All three models predict a similar response as long as damage is restricted to the 90° plies with slightly more degradation predicted by the *periodic crack* model. The onset of angle-ply damage can be noticed in the *Mori-Tanaka* curves as a distinctive kink at $\varepsilon_{xx} \approx 1.5$ ($\beta = 15°$), $\varepsilon_{xx} \approx 0.9$ ($\beta = 30°$), and $\varepsilon_{xx} \approx 0.75$ ($\beta = 40°$). The increased degradation of laminate Poisson's ratio due to angle-ply damage seems to agree well with the experiments. The *constant stress* model also predicts damage in the angle plies starting at a similar axial strain but the angle-ply damage has the opposite effect on the Poisson's ratio. The degradation of laminate Poisson's ratio predicted by the *constant stress* model with angle-ply damage is less than without angle-ply damage. This is a result of the assumption that the degradations of E_2 and G_{12} are equal as illustrated in Fig. 16 by means of the $(\pm 40/90_4)_s$ lay-up. If the degradation of G_{12} is set to 60% of the degradation of E_2 (solid red line in Fig. 16) instead of equal to the degradation of E_2 as before (dashed green line), then the cracking in the angle plies leads to more degradation of the laminate's Poisson's ratio (Fig. 16b) while the change has hardly any effect on the degradation of the laminate's axial modulus (Fig. 16a).

As expected, the two localized damage models do not correlate well with the experimental data in Figs. 12–15 since they are not applicable to the homogeneous loading conditions. The laminate degradation is overestimated since E_2 and G_{12} for the damaged plies are degraded all the way to zero in both models. The leveling of the curves from the `ABAQUS` model signifies complete damage (i.e. $E_2 = G_{12} = 0$) of one type of layer. For $\beta = 0°$ and $\beta = 15°$ (Figs. 12 and 13), the horizontal parts pertain to a fully damaged 90° layer and no damage in the other plies. Figure 14 has two horizontal sections; the small first section corresponds to a fully damaged 90° layer and the second

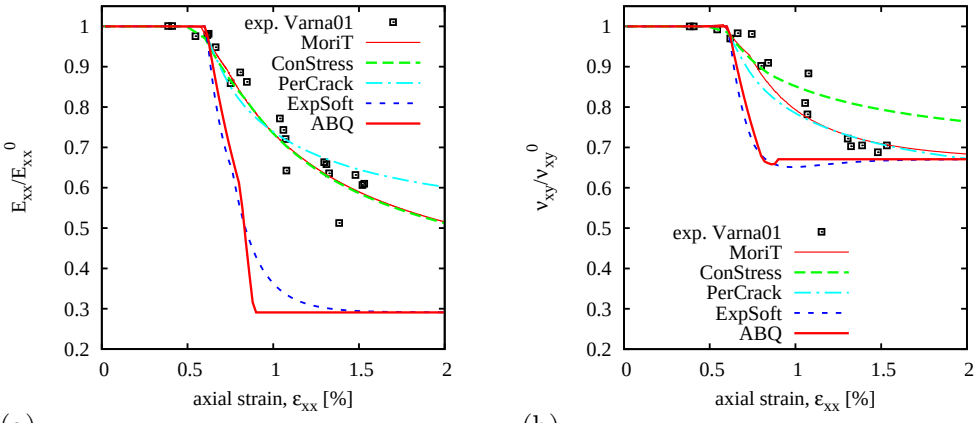

(a) (b)

Fig. 15. Results for lay-up $(\pm 40/90_4)_s$; (a) laminate's axial modulus and (b) Poisson's ratio, normalized by their initial value; experimental data from [29].

horizontal section corresponds to all layers being fully damaged. In Fig. 15, damage in the ±40 layers starts before the 90° layer has been fully degraded, leaving only one horizontal line when all layers have reached their ultimate damage state. Note that for the cases where $\beta = 30°$ and $\beta = 40°$, there is a slight increase of Poisson's ratio with the onset of damage in the angle plies. This is also a result of using the same degradation for E_2 and G_{12}. The responses predicted by the *exponential softening* model are very similar to the `ABAQUS` model predictions except that the progression of the curves is more gradual due to the exponential softening law.

5.2 Laminates type B: off-axis plies $(0/\pm\beta_4/0_{1/2})_s$ *[28]*

The second series of tests was performed on five different laminates with a general $(0/\pm\beta_4/0_{1/2})_s$ lay-up and angles $\beta = 90°, 70°, 55°, 40°, 25°$ [28]. Non-linearity in these laminates originates only from the β-plies which experience various stress ratios, σ_{22}/σ_{12}, depending on the angle β. For shear dominated stress ratios, i.e. $\beta = 40°$ and $\beta = 25°$, no cracking was observed during the experiments [28]. These two tests can therefore only be captured by models containing a non-linear shear formulation such as the *Mori-Tanaka*, the *constant stress*, and the *periodic crack* models. For the first three tests ($\beta = 90°, 70°$, and 55°), on the other hand, the *periodic crack* model cannot be used since it does not allow for cracking in more than one layer and is therefore not applicable to these lay-ups.

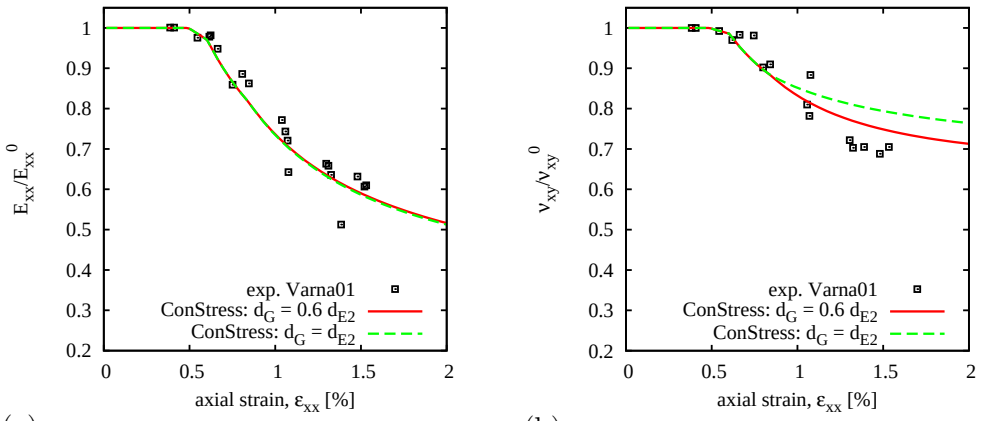

(a) (b)

Fig. 16. Effect of changing the ratio of degradation between E_2 and G_{12} on predictions of the *Constant Stress* model by example of the $(\pm 40/90_4)_s$ lay-up; (a) laminate's axial modulus and (b) Poisson's ratio, normalized by their initial value; experimental data from [29].

Comparisons between the analyses' predictions and experiments are shown in Figs. 17–21. Note that the degradation for $\beta = 90°, 70°$, and $55°$ is given in [28] as a function of crack density, which can be converted to axial strain by analytical curve fits for crack density vs. axial strain which are also provided in [28]. All experimental data points shown for those three lay-ups correspond to crack densities greater than zero. Note that for $\beta = 55°$, the relation between crack density and axial strain varies significantly from specimen to specimen, while the stiffness vs. crack density results are consistent. Therefore, two data sets are derived using a lower bound and an upper bound curve to fit the crack density vs. strain data. This way, the scatter of experimental data is visualized in Fig. 19 by the two data sets for lower bound (lb) and upper bound (ub).

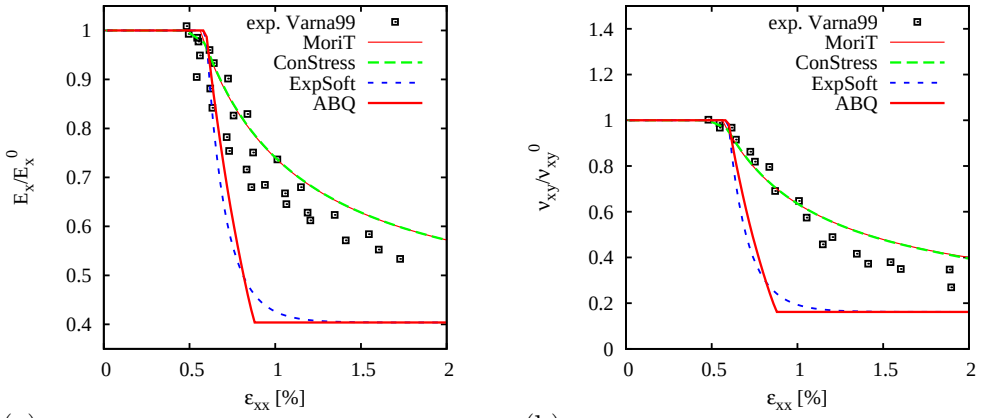

Fig. 17. Results for lay-up $(0/90_8/0_{1/2})_s$; (a) laminate's axial modulus and (b) Poisson's ratio, normalized by their initial value; experimental data from [28].

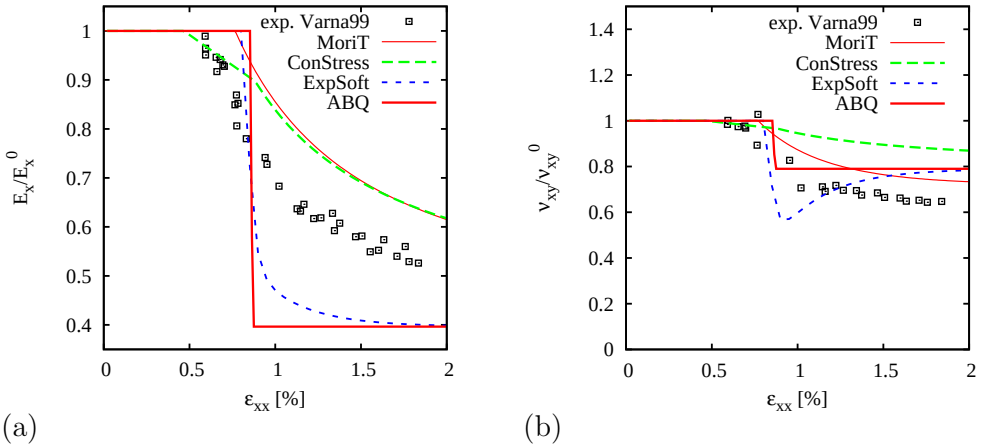

Fig. 18. Results for lay-up $(0/\pm 70_4/0_{1/2})_s$; (a) laminate's axial modulus and (b) Poisson's ratio, normalized by their initial value; experimental data from [28].

The response for $\beta = 90°$ (Fig. 17) is very similar to the first test of the previous test series and confirms the earlier results. In the laminate with $\beta = 70°$ (Fig. 18), cracking during experiments starts below the strains at which the models predict damage onset (the reduction predicted by the *constant stress* model between $\varepsilon_{xx} \approx 0.5$ and $\varepsilon_{xx} \approx 0.8$ is due to plasticity). For $\beta = 55°$ on the other hand, the models unanimously predict damage onset earlier than was observed in the experiments even if the scatter of experimental data is considered (Fig. 19, with lower bound (lb) and upper bound (ub) of experimental data). The reason for this is not quite clear but could be related to matrix plasticity. The test data for the 55° case suggests that there is a significant amount of plasticity involved since the axial stiffness has already decreased prior to damage onset (first point of each experimental data set in Fig. 19).

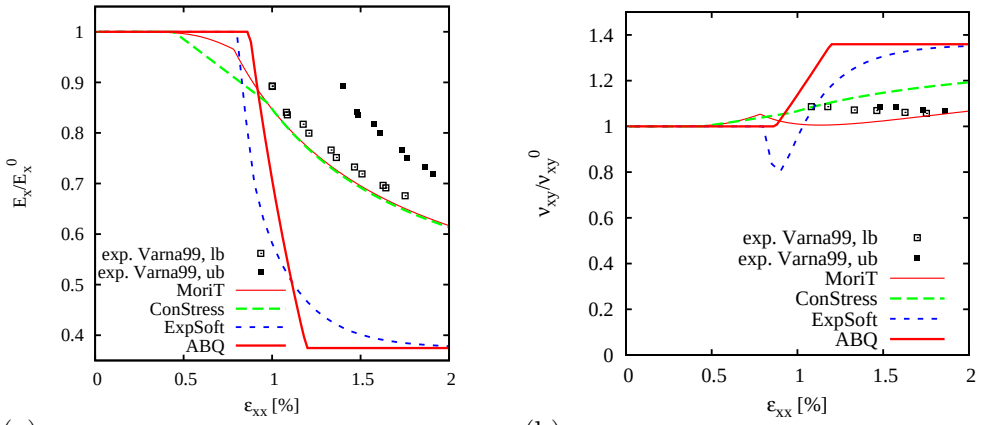

(a) (b)

Fig. 19. Results for lay-up $(0/\pm 55_4/0_{1/2})_s$; (a) laminate's axial modulus and (b) Poisson's ratio, normalized by their initial value; experimental data from [28].

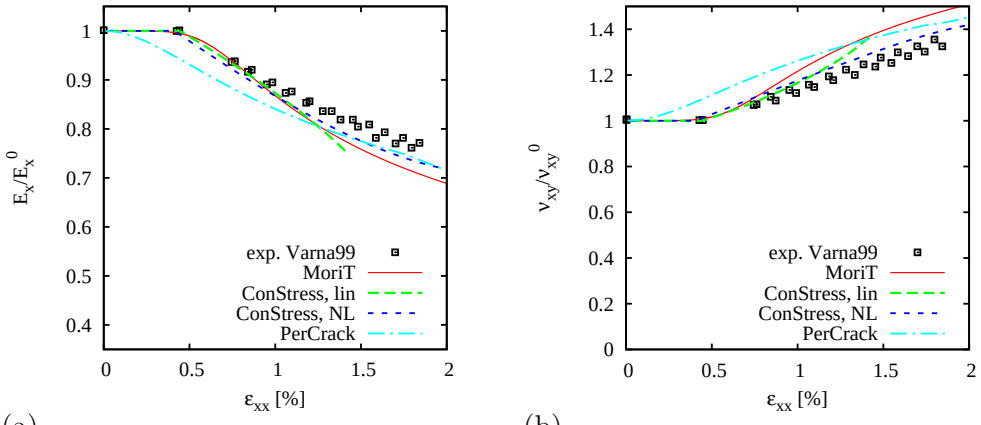

(a) (b)

Fig. 20. Results for lay-up $(0/\pm 40_4/0_{1/2})_s$; (a) laminate's axial modulus and (b) Poisson's ratio, normalized by their initial value; experimental data from [28].

Also the *Mori-Tanaka* and the *constant stress* models predict plastic strains for that laminate. The interaction between plasticity and damage onset will be discussed in more detail in Section 6.

The predicted change in Poisson's ratio for $\beta = 70°$ and $\beta = 55°$ is very sensitive to the exact model formulations. This sensitivity is best explained by reference to the 55° case (Fig. 19b). The *Mori-Tanaka* model predicts a Poisson's ratio increase due to plasticity, but a decrease due to damage. This prediction correlates very well qualitatively with the test data, which also shows an increase prior to damage onset (first data point) and slightly decreases thereafter. The plasticity part of the *constant stress* model predicts a very similar response. However, the damage formulation of that model leads to a further increase of the Poisson's ratio, which results from the assumption that the degradations of E_2 and G_{12} are equal. Since the `ABAQUS` model also uses this assumption, it also predicts the Poisson's ratio to increase with damage but the effect is much more pronounced since degradation is higher in the `ABAQUS` model. In the *exponential softening* model, G_{12} is degraded faster than E_2 for the given material and element size, which leads first to a reduction of ν_{xy}. Ultimately, the ply stiffnesses E_2 and G_{12} are both reduced to zero, and the prediction converges to that of the `ABAQUS` model.

The angle plies of the last two lay-ups ($\beta = 40°$ and $\beta = 25°$ in Figs. 20 and 21, respectively) experience a very small stress ratio σ_{22}/σ_{12} and do not show any damage in the strain range considered. The non-linear elastic function used by the *periodic crack* model for the non-linear shear response predicts too much non-linearity at low strains, but gives good results at higher strains. The predictions of the *Mori-Tanaka* and the *constant stress* models are very similar up to $\varepsilon_{xx} \approx 1\%$. Up to that strain, the non-linear shear response is known from experiments (see Fig. 4). For $\varepsilon_{xx} > 1\%$, the plasticity law has to

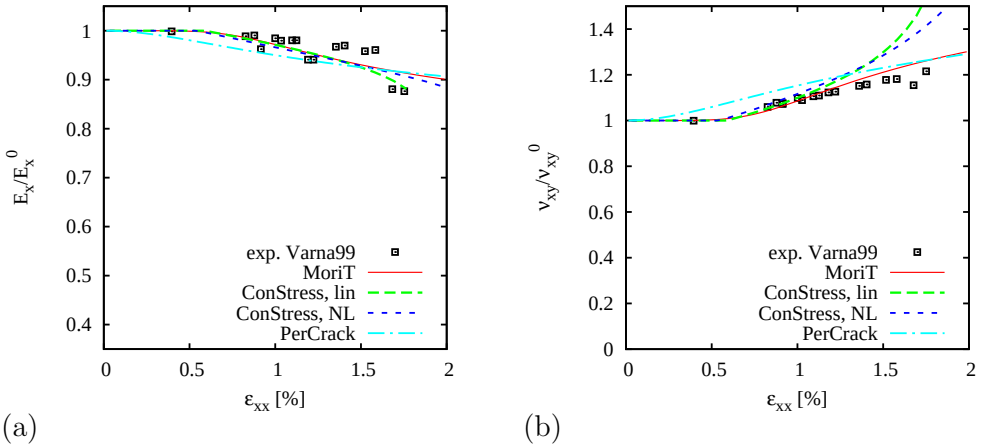

(a) (b)

Fig. 21. Results for lay-up $(0/\pm 25_4/0_{1/2})_s$; (a) laminate's axial modulus and (b) Poisson's ratio, normalized by their initial value; experimental data from [28].

be extrapolated. The extrapolation used for the *Mori-Tanaka* model correlates quite well with the experimental data. For the *constant stress* model, the linear extrapolation gives good results for the laminate's axial stiffness but leads to an overprediction of Poisson's ratio at $\varepsilon_{xx} > 1.5\%$. Changing to a non-linear extrapolation improves the Poisson's ratio predictions only slightly.

6 DISCUSSION AND CONCLUSIONS

In the present study, five different damage models are evaluated for matrix dominated loading conditions and are compared both qualitatively and quantitatively. The emphasis is laid on predicting the effects of distributed damage in an embedded ply typically caused by fairly homogeneous stress states. Three of the damage models considered are specifically designed for damage under homogeneous loading, while the other two are localized damage models. Although the localized damage models are not intended for modeling distributed matrix cracking, they are also included in this study for comparison.

In general, the three distributed damage models correlate well with the experimental data shown here. However, none of the models captures all of the non-linear effects. Based on comparisons of the models' predictions to experimental data of uniaxial tension specimens with various lay-ups, several lessons can be learned.

Non-linearity without damage (plasticity)

Experimental data shows that the response of a laminate can be non-linear prior to matrix cracking, especially under shear dominated loading conditions. The origin of this non-linear behavior is still disputed but could be due to matrix plasticity. The *Mori-Tanaka* and the *constant stress* models assume plasticity laws while the *periodic crack* model uses a non-linear elastic formulation. However, since only monotonic loading was considered here, the validity of either plastic or elastic unloading was not investigated.

All three models for distributed damage capture the non-linear shear response based on curve fits of experimental data. Consequently, the agreement between predictions and experiments only depends on the quality of the curve fit. The expressions used by the *Mori-Tanaka* and the *constant stress* models capture the non-linear shear response very well, while the *periodic crack* model overpredicts the amount of non-linearity at low strains. Note that the correlation of the *periodic crack* model could easily be improved by using a higher exponent in the curve-fit equation.

For some of the test cases considered, the non-linear shear response needs to be extrapolated. The equations used by the *Mori-Tanaka* and the *periodic crack* models yield good results, even at high shear strains where extrapolation is necessary. For the *constant stress* model, a linear relation between secant shear modulus and equivalent strain has been suggested. Although the linear approximation matches experimental data at low strains, a non-linear extrapolation is needed at higher strains.

While the *Mori-Tanaka* and the *periodic crack* models assume non-linearity prior to damage to occur only due to shear stresses, the *constant stress* model also postulates a non-linear response under transverse tension, even though non-linearity is not observed in transverse tension tests of UD-laminates. This assumption is reasonable for the following reasons. If the non-linearity observed under shear is a result of plasticity in the matrix, transverse tension should also result in plasticity due to the deviatoric part of the strain tensor. However, this effect is difficult to measure experimentally, since it only occurs in embedded plies as a result of the increased in-situ strength. A UD-laminate typically fails at lower stresses than the same ply embedded in a laminate, and therefore, does not exhibit any non-linearity prior to failure. Note that the test data for laminates with embedded 90° plies show a small amount of non-linearity prior to damage onset, which could be an indication of plasticity. However, the effect is very small and further study is necessary to draw any firm conclusions.

Damage initiation

The damage initiation criteria used by the five models for matrix tension are very similar. The main difference lies in the definition of the stresses that are used to evaluate the initiation functions. The *Mori-Tanaka* model uses the nominal ply stress state, which is a function of the damage state, and requires iteration inside the material subroutine to determine the state variables. All other models use an effective stress and do not require iteration. However, in specific cases this approach can lead to results that are inconsistent with experimental observations (depending on the definition of the effective stresses).

As indicated by the test cases with off-axis plies, the prediction of damage onset under multi-axial stress states remains the primary challenge, since none of the initiation criteria predict damage onset in the off-axis plies correctly. Strains at damage onset are overpredicted for $\beta = 70°$ and underpredicted for $\beta = 55°$. The reason for this discrepancy is not clear. A possible explanation is the effect of matrix plasticity. When plasticity in the matrix is an issue, the stress–strain curve becomes very flat such that a large increase in strain leads only to a small increase in stress. As a result, damage initiation is relatively insensitive to variations in strain since damage initiation is triggered by stress

based criteria. This has two implications. First, it explains the large scatter of experimental failure strains for the $\beta = 55°$ test. Second, both the stress state and the ply strength need to be known very accurately in order to correctly predict damage onset in a model and this requires an adequate plasticity formulation and reliable failure criteria for multi-axial stress states.

Another issue is the effect of plasticity on the perceived strength of an embedded ply. When the in-situ effect is studied in experiments, only the strain state at failure is known and the ply's failure stress has to be computed based on an assumed ply constitutive law. As discussed above, there are several indications that an embedded ply experiences plastic deformations, even under transverse tensile loading. However, the in-situ strength under transverse tension is typically determined based on a linear-elastic transverse response, thereby leading to higher transverse stresses and a higher perceived in-situ strength. From these considerations, it is clear that the constitutive behavior of a ply has to be fully understood, both from the modeling and the experimental perspective, in order to improve the prediction of damage onset.

Strain softening

The test data of uni-axial tension tests on cross-ply laminates show that damage under transverse tension leads to strain softening but the ply stresses do not vanish completely in the strain range considered. This response is captured best by the *periodic crack* model as long as cracking occurs in one layer only (as assumed in the formulation of the model). The *Mori-Tanaka* and the *constant stress* models assume no softening due to damage which does not agree that well with experiments. However, the error in the predicted overall response of a multi-axial laminate is small enough to be acceptable for most practical purposes. Since a non-softening constitutive law is easier to handle from a numerical point of view, the better accuracy of a model with strain softening should be weighted against the higher computational effort.

Property degradation

The longitudinal Young's modulus and the major Poisson's ratio of a ply are not affected by matrix cracking if the fibers are perfectly aligned and the matrix cracks are perfectly thin. All models considered here generally concur in this assumption. In the *Mori-Tanaka* model, the property degradation is controlled by the aspect ratio of the Mori-Tanaka inclusions. If the aspect ratio approaches zero, E_1 and ν_{12} remain constant, independently of the damage state. For a slightly higher aspect ratio, E_1 is degraded and ν_{12} increases with damage, which qualitatively may give better correlation with experimental

data if the fibers in a ply are not perfectly aligned. However, variation of the aspect ratio was not investigated in the present study.

Based on comparison of model predictions to experimental data of tensile tests on various laminates, there is little difference between the predictions of the three distributed damage models for the degradation of laminate axial modulus. The predicted changes of the laminates' Poisson's ratios with damage, however, point out some differences in the model formulations. The predicted values of Poisson's ratio qualitatively show better correlation with experiments for those models where the degradation of a ply's transverse Young's modulus is larger than the degradation of the shear modulus (*Mori-Tanaka* and *periodic crack*). The *constant stress* model assumes equal degradation of Young's modulus and shear modulus, which can have an effect on the laminate Poisson's ratio that is opposite to that shown by test data (results for $\beta = 30°$ and $\beta = 40°$ in Section 5.1 and $\beta = 55°$ in Section 5.2).

The observation that the Poisson's ratio is much more sensitive to the different model formulations also emphasizes the importance of gathering as much information as possible during experimental testing. Looking only at the change in axial modulus, there is little difference between predictions from the three distributed damage models. The comparisons of Poisson's ratio, on the other hand, give some important clues as to which model assumptions capture the actual material response more realistically.

Localized damage

The test cases considered in this study are concerned with homogeneous stress states that lead to distributed damage. However, failure in composite structures is often triggered near stress concentrations which can lead to localized cracks, usually combined with delamination near the intersection between the crack and the ply interface. The *exponential softening* model and the `ABAQUS` model are designed to model localized cracking. Since most structures have homogeneously loaded areas and geometric features resulting in stress concentrations, the optimal damage model would be a constitutive law that is able to distinguish between these two situations and predict the response accordingly. However, that would require a non-local formulation of the constitutive law which is difficult to realize within the framework of commercial FEM software.

One alternative is to use models for localized damage throughout the structure even though their predictions in homogeneously loaded areas will be less accurate. Applying the two localized damage models to the test cases in this study shows that the effect of matrix damage in general is overpredicted and, depending on the laminate lay-up, the error can be quite high. In addition, the *exponential softening* model and the `ABAQUS` model do not include any

plasticity formulations and therefore do not capture the response under shear dominated loading very well. However, the laminates studied here were designed to emphasize the effect of matrix damage such that it could be studied properly. Laminates for practical applications usually have more evenly distributed fiber directions (e.g. quasi-isotropic laminates) and thinner ply groups so the error in the predicted laminate stiffness would be smaller. Furthermore, the predictions can be considered a conservative estimate. It should also be kept in mind that the main purpose of these models is to predict ultimate failure. In practical applications, especially when quasi-isotropic laminates are used, ultimate failure is typically dominated by fiber failure while the exact matrix response is often less relevant.

Acknowledgement

This research was supported by the NASA Postdoctoral Program at NASA Langley Research Center, administered by Oak Ridge Associated Universities.

REFERENCES

[1] Allen, D. H., 1994. Damage evolution in laminates. In Talreja, R., editor, *Damage Mechanics of Composite Materials*, vol. 9 of *Composite Materials Series*, chap. 3. Elsevier Science Ltd., Oxford, UK.

[2] Barbero, E. J., Lonetti, P., 2002. An inelastic damage model for fiber reinforced laminates. J. Comp. Mat. 36, 941–962.

[3] Joffe, R., Krasnikovs, A., Varna, J., 2001. COD-based simulation of transverse cracking and stiffness reduction in $[S/90_n]_s$ laminates. Comp. Sci. and Tech. 61, 637–656.

[4] Ladevèze, P., 2001. A damage mesomodel of laminate composites. In Lemaitre, J., editor, *Handbook of Materials Behavior Models*, 1004–1014. Academic Press, London, UK.

[5] Mayugo, J. A., Camanho, P. P., Maimí, P., Dávila, C. G., 2006. A micromechanics-based damage model for $[\pm\theta/90_n]_{\mathrm{s}}$ composite laminates. Tech. Rep. TM-2006-214285, NASA.

[6] Mayugo, J. A., Camanho, P. P., Maimí, P., Dávila, C. G., 2010. Analytical modelling of transverse matrix cracking of $[\pm\theta/90_n]_{\mathrm{s}}$ composite laminates under multiaxial loading. Mech. Adv. Mater. Struct. 17, 237–245.

[7] Maimí, P., Camanho, P. P., Mayugo, J. A., Dávila, C. G., 2007. A continuum damage model for composite laminates. Part I: Constitutive model. Mech. Mat. 39, 897–908.

[8] Maimí, P., Camanho, P. P., Mayugo, J. A., Dávila, C. G., 2007. A continuum damage model for composite laminates. Part II: Computational implementation and validation. Mech. Mat. 39, 909–919.

[9] Lapczyk, I., Hurtado, J. A., 2007. Progressive damage modeling in fiber-reinforced materials. Composites Part A 38, 2333–2341.

[10] Schuecker, C., Dávila, C. G., Pettermann, H. E., 2008. Modeling the non-linear response of fiber-reinforced laminates using a combined damage/plasticity model. Tech. Rep. TM-2008-215314, NASA.

[11] Schuecker, C., Pettermann, H. E., 2008. Combining elastic brittle damage with plasticity to model the non-linear behavior of fiber reinforced laminates, vol. 10 of *Computational Methods in Applied Sciences*, chap. 5, 99–117. Springer. ISBN: 978-1-4020-8583-3.

[12] Pinho, S. T., Robinson, P., Schuecker, C., Camanho, P. P. Pressure-depedent constitutive and failure model for laminated composites. In *Proceedings of the 17th International Conference on Composite Materials (ICCM17), 27-31 July, 2009, Edinburgh, UK*. Extended version *Material and structural response of polymer-matrix fibre-reinforced composites* accepted for publication for the World Wide Failure Exercise, Part II.

[13] Puck, A., Schürmann, H., 1998. Failure analysis of FRP laminates by means of physically based phenomenological models. Comp. Sci. and Tech. 58, 1045–1067.

[14] Pinho, S. T., Dávila, C. G., Camanho, P. P., Iannucci, L., Robinson, P., 2005. Failure models and criteria for FRP under in-plane or three-dimensional stress states including shear non-linearity. Tech. Rep. TM-2005-213530, NASA.

[15] Puck, A., 1996. Festigkeitsanalyse von Faser-Matrix-Laminaten. Carl Hanser Verlag, München Wien, Germany.

[16] Schuecker, C., Pahr, D. H., Pettermann, H. E., 2006. Accounting for residual stresses in FEM analyses of laminated structures using the Puck criterion for three-axial stress states. Comp. Sci. and Tech. 66, 2054–2062.

[17] Mori, T., Tanaka, K., 1973. Average stress in the matrix and average elastic energy of materials with misfitting inclusions. Acta Metall. 21, 571–574.

[18] Camanho, P. P., Mayugo, J. A., Maimí, P., Dávila, C. G., 2006. A micromechanics-based damage model for the strength prediction of composite laminates. In *Proc. of European Conference on Computational Mechanics (ECCM 2006), June 5–9, 2006, Lisbon, Portugal*. Paper 1661.

[19] Nuismer, R. J., Tan, S. C., 1988. Constitutive relations of a cracked composite lamina. J. Comp. Mat. 22, 306–321.

[20] Tan, S. C., Nuismer, R. J., 1989. A theory for progressive matrix cracking in composite laminates. J. Comp. Mat. 23, 1029–1047.

[21] Hahn, H. T., 1983. A mixed-mode fracture criterion for composite materials. Composites Technology Review 5, 26–29.

[22] Camanho, P. P., Dávila, C. G., Pinho, S. T., Iannucci, L., Robinson, P., 2006. Prediction of in situ strengths and matrix cracking in composites under transverse tension and in-plane shear. Composites Part A 37, 165–176.

[23] Bažant, Z. P., Oh, B. H., 1983. Crack band theory for fracture of concrete. Materials & Structures 16, 155–177.

[24] ABAQUS/Standard User's Manual, Version 6.7. ABAQUS Inc., Pawtucket, RI, USA.

[25] Hashin, Z., 1980. Failure criteria for unidirectional fiber composites. J. Appl. Mech. 47, 329–334.

[26] Puck, A., Kopp, J., Knops, M., 2002. Guidelines for the determination of the parameters in Puck's action plane strength criterion. Comp. Sci. and Tech. 62, (3) 371–378; (9) 1275.

[27] Joffe, R., Varna, J., 1999. Analytical modeling of stiffness reduction in symmetric and balanced laminates due to cracks in 90° layers. Comp. Sci. and Tech. 59, 1641–1652.

[28] Varna, J., Joffe, R., Akshantala, N. V., Talreja, R., 1999. Damage in composite laminates with off-axis plies. Comp. Sci. and Tech. 59, 2139–2147.

[29] Varna, J., Joffe, R., Talreja, R., 2001. A synergistic damage-mechanics analysis of transverse cracking in $[\pm\theta/90_4]_s$ laminates. Comp. Sci. and Tech. 61, 657–665.

[30] Soden, P. D., Hinton, M. J., Kaddour, A. S., 1998. Lamina properties, lay-up configurations and loading conditions for a range of fibre-reinforced composite laminates. Comp. Sci. and Tech. 58, 1011–1022.

[31] Parvizi, A., Garrett, K., Bailey, J., 1978. Constrained cracking in glass fiber reinforced epoxy cross-ply laminates. J. Mat. Sci. 13, 195–201.

[32] Crossman, F. W., Warren, W. J., Wang, A. S. D., Law Jr., G. E., 1980. Initiation and growth of transverse cracks and edge delamination in composite laminates, part 2: Experimental results. J. Comp. Mat. 14, 88–108.

[33] Flaggs, D. L., Kural, M. H., 1982. Experimental determination of the in situ transerse lamina strength in graphite/epoxy laminates. J. Comp. Mat. 16, 103–16.

[34] Chang, F. K., Chen, M. H., 1987. The in situ ply shear strength distributions in graphite/epoxy laminated composites. J. Comp. Mat. 21, 708–33.

[35] Schuecker, C., 2005. Mechanism based modeling of damage and failure in fiber reinforced polymer laminates. Ph.D. thesis, Institute of Lightweight Design and Structural Biomechanics, Vienna University of Technology, Vienna, Austria. (also published in: VDI Fortschritt-Berichte VDI Reihe 18 Nr. 303. VDI-Verlag, Düsseldorf).

[36] Pettersson, K., 2005. The Inclined Double Notch Shear Test for Determination of Interlaminar Shear Properties of Composite Laminates. Ph.D. thesis, Royal Institute of Technology, Solid Mechanics, Stockholm, Sweden.

[37] Van Paepegem, W., De Baere, I., Degrieck, J., 2006. Modelling the nonlinear shear stress–strain response of glass fibre-reinforced composites. Part I: Experimental results. Comp. Sci. and Tech. 66, 1455–1464.

[38] Yang, G., Cox, B., 2005. Cohesive models for damage evolution in laminated composites. Int. J. Fracture 133, 107–137.

REPORT DOCUMENTATION PAGE

Form Approved
OMB No. 0704-0188

1. REPORT DATE *(DD-MM-YYYY)*	2. REPORT TYPE	3. DATES COVERED *(From - To)*
01- 10 - 2010	Technical Publication	

4. TITLE AND SUBTITLE

Comparison of Damage Models for Predicting the Non-linear Response of Laminates Under Matrix Dominated Loading Conditions

5a. CONTRACT NUMBER

5b. GRANT NUMBER

5c. PROGRAM ELEMENT NUMBER

6. AUTHOR(S)

Schuecker, Clara; Dávila, Carlos G.; Rose, Cheryl A.

5d. PROJECT NUMBER

5e. TASK NUMBER

5f. WORK UNIT NUMBER

698259.02.07.07.03.03

7. PERFORMING ORGANIZATION NAME(S) AND ADDRESS(ES)

NASA Langley Research Center
Hampton, VA 23681-2199

8. PERFORMING ORGANIZATION REPORT NUMBER

L-19916

9. SPONSORING/MONITORING AGENCY NAME(S) AND ADDRESS(ES)

National Aeronautics and Space Administration
Washington, DC 20546-0001

10. SPONSOR/MONITOR'S ACRONYM(S)

NASA

11. SPONSOR/MONITOR'S REPORT NUMBER(S)

NASA/TP-2010-216856

12. DISTRIBUTION/AVAILABILITY STATEMENT

Unclassified - Unlimited
Subject Category 24
Availability: NASA CASI (443) 757-5802

13. SUPPLEMENTARY NOTES

14. ABSTRACT

Five models for matrix damage in fiber reinforced laminates are evaluated for matrix-dominated loading conditions under plane stress and are compared both qualitatively and quantitatively. The emphasis of this study is on a comparison of the response of embedded plies subjected to a homogeneous stress state. Three of the models are specifically designed for modeling the non-linear response due to distributed matrix cracking under homogeneous loading, and also account for non-linear (shear) behavior prior to the onset of cracking. The remaining two models are localized damage models intended for predicting local failure at stress concentrations. The modeling approaches of distributed vs. localized cracking as well as the different formulations of damage initiation and damage progression are compared and discussed.

15. SUBJECT TERMS

Matrix cracks; Continuum damage models; Composites; Fiber reinforced laminates; Polymer matrix composites; Computational mechanics; Non-linear modeling; Continuum damage; Plasticity

16. SECURITY CLASSIFICATION OF:			17. LIMITATION OF ABSTRACT	18. NUMBER OF PAGES	19a. NAME OF RESPONSIBLE PERSON
a. REPORT	b. ABSTRACT	c. THIS PAGE			STI Help Desk (email: help@sti.nasa.gov)
					19b. TELEPHONE NUMBER *(Include area code)*
U	U	U	UU	43	(443) 757-5802